Subjective Vertical Conflict Model With Visual Vertical: Predicting Motion Sickness on Autonomous Personal Mobility Vehicles

Hailong Liu, *Member, IEEE*, Shota Inoue, and Takahiro Wada, *Member, IEEE*

***Abstract*— Passengers of level 3-5 autonomous personal mobility vehicles (APMV) can perform non-driving tasks, such as reading books and smartphones, while driving. It has been pointed out that such activities may increase motion sickness, especially when frequently avoiding pedestrians or obstacles in shared spaces. Many studies have been conducted to build countermeasures, of which various computational motion sickness models have been developed. Among them, models based on subjective vertical conflict (SVC) theory, which describes vertical changes in direction sensed by human sensory organs v.s. those expected by the central nervous system, have been actively developed. To model motion sickness due to conflict between visual vertical information and vestibular sensation, we proposed a 6 DoF SVC-VV model which added a visually perceived vertical block into a conventional 6 DoF SVC model to predict visual vertical directions from image data simulating the visual input of a human. In a driving experiment, 27 participants rode on the APMV and experienced slalom driving with two visual conditions: looking ahead (LAD) and working with a tablet device (WAD). We verified that passengers got motion sickness while riding the APMV, and the symptoms were severer when especially working on it, by simulating the frequent pedestrian avoidance scenarios of the APMV in the experiment. In addition, the results of the experiment demonstrated that the proposed 6 DoF SVC-VV model could describe the increased motion sickness experienced when the visual vertical and gravitational acceleration directions were different.**

***Index Terms*— Motion sickness, subjective vertical conflicts, riding comfort, autonomous personal mobility vehicles.**

I. Introduction

LEVEL 3-5 of driving automation [1] are applied to cars and miniaturized personal mobility vehicles (PMVs) [2], [3]. Autonomous PMVs (APMVs) are expected to be widely used in mixed traffic and shared space conditions, such as sidewalks, shopping centers, stations, and school campuses [4], [5], [6]. Additionally, drivers (passengers) of AVs (including APMVs) are allowed to perform non-driving tasks during autonomous driving [7], [8], [9], [10], e. g., reading a book [11], [12], [13], watching videos [11], [14], and playing games [15], [16]. Unfortunately, the above usage scenarios pose a potential risk of motion sickness for passengers on the APMV by the following reasons:

1) In these mixed traffic environments, other traffic participants such as pedestrians, bicycles, and other vehicles, will frequently interact with AVs (including APMVs) [13], [17]. Passengers may be prone to motion sickness owing to the lack of control of the APMV and passive body movement [7], [8], [9], [18] when the APMV does avoidance behaviors frequently.
2) Motion sickness may occur with a high probability when the visual and vestibular systems are stimulated with incongruent information [9], [19].

Based on the aforementioned issues, preventing motion sickness can be considered an important challenge for the popularity and widespread use of APMVs. To address these issues, various computational models have been used to evaluate or estimate the severity of motion sickness.

A. Related Works

The sensory conflict (SC) theory is widely used to explain the mechanism of motion sickness, which postulates that motion sickness is caused by conflicts between one sensory and expected signals based on previous experience [19]. Oman proposed a mathematical model of the SC theory based on an observer or optimal estimation theoretic framework, in which motion perception was assumed to be influenced or corrected by the discrepancy between signals from sensory organs and those calculated by internal models in our central nervous systems, and the discrepancy is regarded as a conflict in the SC theory [20].

Based on SC theory, Bles et al. [21] proposed the subjective vertical conflict (SVC) theory, which postulates that motion sickness is caused by conflict between the vertical directions sensed by sensory organs and those estimated by the central nervous systems or their internal models. Moreover, Bos and Bles [22] proposed the first computational motion sickness model of the SVC theory. This model simulates the process of motion sickness caused by conflicts between otolith organs (OTO) and their internal models using one-degree-of-freedom (1 DoF) vertical acceleration inputs. To express

Manuscript received 21 February 2023; revised 6 November 2023 and 14 January 2024; accepted 18 January 2024. Date of publication 7 February 2024; date of current version 1 August 2024. This work was supported by the Japan Society for the Promotion of Science (JSPS) KAKENHI, Japan, under Grant 21K18308 and Grant 21H01296. The Associate Editor for this article was S. A. Birrell. *(Corresponding author: Hailong Liu.)*

This work involved human subjects in its research. Approval of all ethical and experimental procedures and protocols was granted by the Research Ethics Committee of Nara Institute of Science and Technology, Japan, under Application No. 2021-I-38.

The authors are with the Graduate School of Science and Technology, Nara Institute of Science and Technology, Ikoma, Nara 630-0192, Japan (e-mail: liu.hailong@is.naist.jp).

Digital Object Identifier 10.1109/TITS.2024.3357170

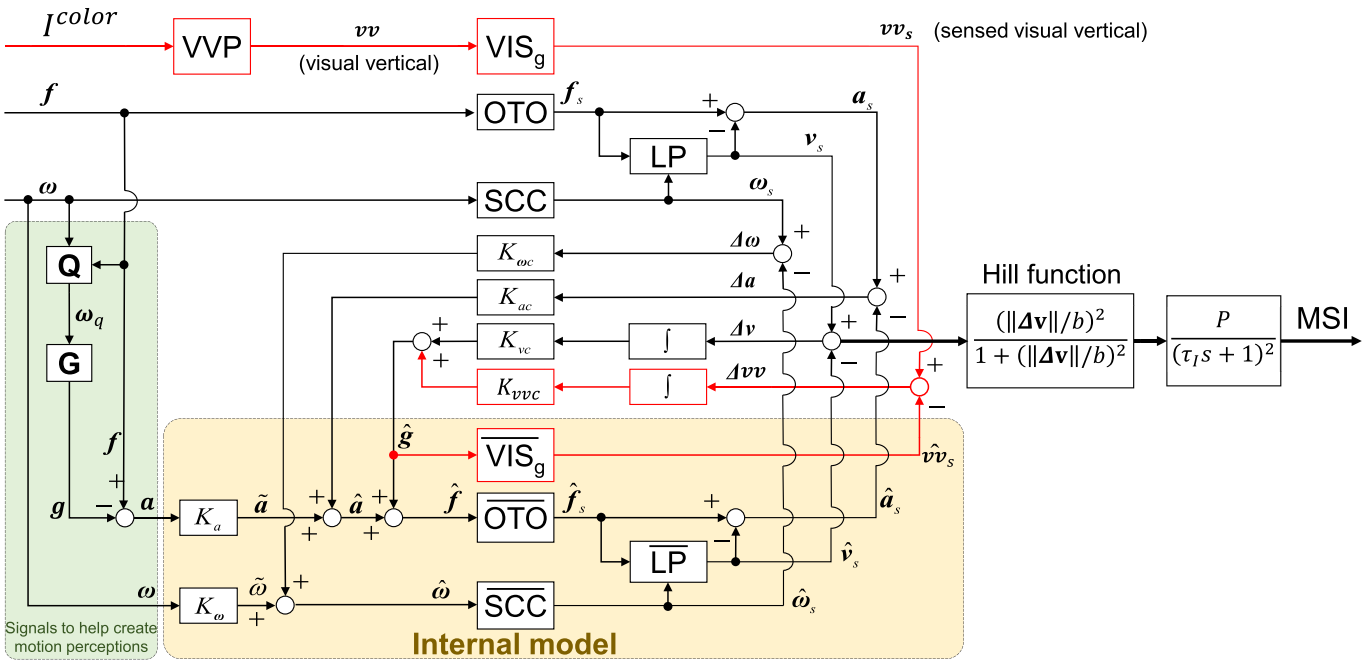

Fig. 1. Proposed 6 DoF SVC-VV model: motion sickness computational model considering the vertical sensed using vestibular-visual interactions.

motion sickness caused by multiple degrees-of-freedom of head movement, including head rotation, Kamiji et al. [23] extended the 1 DoF SVC model [22] to a six-degrees-of-freedom (6 DoF) SVC model, which included the OTO and semi-circular canals (SCC) in the vestibular system to accept the three-dimensional (3D) acceleration and 3D angular velocity inputs. Moreover, based on the Kamiji et al. [23]'s 6 DoF SVC model, Inoue et al. [24] optimized the structures of conflict feedback integration and parameters to increase the accuracy of the 6 DoF SVC model in presenting the tendency of motion sickness and motion perception of verticality.

Furthermore, Bos et al. [25] suggested that visually induced motion sickness can also be explained by SVC theory and proposed a model framework that includes visual information such as visual angular velocities and visual vertical (VV) information. However, this study did not consider a concrete method for the application of the experimental data. As a computational model of motion sickness that can address visual–vestibular interactions, Braccesi and Cianetti [26] proposed a motion sickness model based on the interaction between the OTO and visual acceleration. However, this model does not consider the rotation of the head as perceived by the SCC and visual perception. To address this issue, Wada et al. [27] expanded the original 6 DoF SVC model Kamiji et al. [23] for vestibular motion sickness to include visual-based angular velocity perception using the optical flow method from camera images.

Recalling SVC theory, motion sickness is primarily caused by a conflict of vertical perception between sensor organs and their internal models. Moreover, some medical studies point to a correlation between the disability in vertical visual perception and motion sickness [28], [29], [30]. Therefore, based on Kamiji et al. [23]'s work, we proposed a 6 DoF SVC-VV model that represents motion sickness owing to the vertical perception from interactions of visual-vestibular systems in our preliminary work [13]. However, in this pre-study, we did not compare the predicted results using the model with the participants' feelings of motion sickness. Moreover, we only verified the accuracy of the proposed visual vertical prediction method in a wide outdoor environment; its performance in complex indoor environments remains uncertain.

B. Purposes and Contributions

There are two purposes of this study. The first one is to confirm that frequent avoidance behaviors of APMV will cause its passengers getting motion sickness. The second one is to propose a motion sickness computational model based on the SVC theory which addresses the vertical perception and visual-vestibular interaction.

Therefore, the contributions of this study are as follows:

1) We verified that passengers got motion sickness while riding the APMV, particularly working on it, by simulating the frequent pedestrian avoidance scenarios of the APMV in the subject's experiment.
2) A 6 DoF SVC-VV model was proposed based on the conventional 6 DoF SVC model [24], which represents motion sickness owing to the vertical perception from interactions of visual-vestibular systems.
3) We verified that the proposed 6 DoF SVC-VV model has a performance to represent the increase in motion sickness caused by passengers working with tablet devices while riding in APMV.

II. Motion Sickness Modeling With Visual Vertical Estimation

In this study, we propose a 6 DoF SVC-VV model to predict motion sickness incidence (MSI) considering vestibular-visual interaction, as shown in Fig. 1. This model adds the visual vertical (VV) estimation (shown as red paths) into the 6 DoF

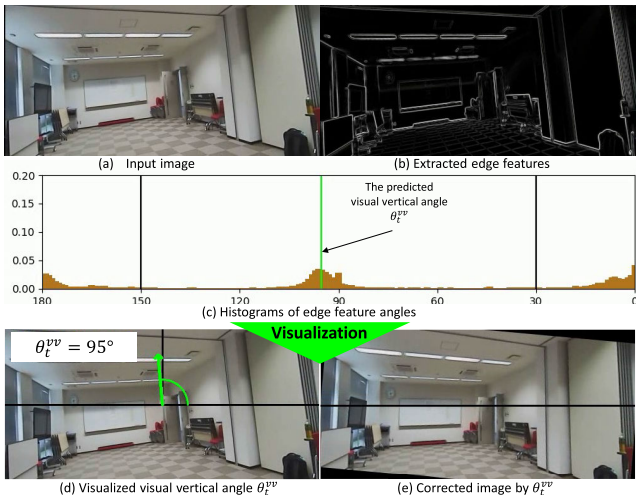

Fig. 2. An example shows the process of visual vertical prediction in (a)-(c). Visualization results of the predicted visual vertical are shown in (d) and (e).

SVC model proposed by [24] (shown as black paths). Moreover, we improve this model to reduce the negative impact of measurement errors in the actual experiment. In this section, the methods for modeling the visual vertical perception, vestibular system, and interactions with their internal models are presented separately.

A. Visual Vertical Prediction Modeling

Considering that the visual vertical (VV) is thought to be derived from signals presumed to be parallel or perpendicular to vertical objects, such as buildings or the horizon in the environment [31], a simple image processing method is proposed to estimate the visual vertical by analyzing the directions of the edges of objects in images in our pre-study [13]. In this pre-study, we only considered the usage of APMV in open outdoor areas; thus, the visual vertical direction was calculated based on horizontal edge features such as the horizon and horizontal edge of the building. However, in indoor scenes with various obstacles such as tables, chairs, and benches, the horizontal edge features change with the viewing angle because of the visual perspective, particularly in frequent avoidance behaviors of APMV. Therefore, we take the vertical edge features, e. g., edges of columns and window frames to calculate the visual vertical direction in this study. An example of visual vertical prediction and visualization of the predicted visual vertical is shown in Fig. 2. The details of the visual vertical prediction are described as follows.

The VVP block shown in Fig. 1 represents the process of the visual system predicting the visual vertical from an image. The proposed visual vertical prediction method is shown in Algorithm 1. The input is a $\boldsymbol{I}_t^{color} \in \mathbb{R}^{H\times W\times 3}$ which is defined as a color image in the t-th frame captured by a camera attached to the human head (see Fig. 8) to imitate human visual input (see Fig. 2 (a)). Then, $\boldsymbol{I}_t^{color}$ is preprocessed by converting to a gray-scale image and normalizing through the global maximum and minimum (Algorithm 1, steps 1-2).

Subsequently, Sobel operators are used to calculate the gradients in the horizontal direction $\nabla \boldsymbol{x}_t$ and vertical direction $\nabla \boldsymbol{y}_t$ in the image coordinate system to detect the edges of objects in the image (Algorithm 1, steps 3-4). The gradient

Algorithm 1 Visual Vertical Direction Estimation Method for VVP Block in Fig. 1.

Input: $\boldsymbol{I}_t^{color} \in \mathbb{R}^{H\times W\times 3}$ and $\theta_0^{vv} = 90$,
where $H = 400$, $W = 1000$, $t \in \{1, \cdots T\}$
Output: θ^{vv}

1: $\boldsymbol{I}_t^{gray} \in \mathbb{R}^{H\times W} \leftarrow \mathrm{Gray}(\boldsymbol{I}^{color})$
2: $\boldsymbol{I}_t^{gray} \in \mathbb{R}^{H\times W} \leftarrow \mathrm{Normalization}_{min}^{max}(\boldsymbol{I}_t^{gray})$
3: $\nabla \boldsymbol{x}_t \in \mathbb{R}^{H\times W} \leftarrow \mathrm{Sobel}_x(\boldsymbol{I}_t^{gray})$
4: $\nabla \boldsymbol{y}_t \in \mathbb{R}^{H\times W} \leftarrow \mathrm{Sobel}_y(\boldsymbol{I}_t^{gray})$
5: $\boldsymbol{M}_t = (\nabla \boldsymbol{x}_t \odot \nabla \boldsymbol{x}_t + \nabla \boldsymbol{y}_t \odot \nabla \boldsymbol{y}_t)^{\odot 1/2}$
6: $\Theta_t = (180/\pi)\arctan(\nabla \boldsymbol{x}_t \oslash \nabla \boldsymbol{y}_t)$
7: **for** $i = 0$ to H **do**
8: **for** $j = 0$ to W **do**
9: $$(\Theta_t)_{i,j} \leftarrow \begin{cases} (\Theta_t)_{i,j} & (0 \le (\Theta_t)_{i,j} < 180) \\ (\Theta_t)_{i,j} - 180 & (180 \le (\Theta_t)_{i,j} < 360) \\ 0 & ((\Theta_t)_{i,j} = 360) \end{cases}$$
10: **end for**
11: **end for**
12: $\boldsymbol{M}_t \leftarrow \mathrm{Normalization}_{min}^{max}(\boldsymbol{M}_t)$
13: **for** $d = 0$ to 179 **do**
14: $(\boldsymbol{\theta}_t^{hist})_d \leftarrow \sum_{i=0}^{H}\sum_{j=0}^{W} \mathbf{1}_d[(\Theta_t)_{i,j}](\boldsymbol{M}_t)_{i,j}$,
where $\boldsymbol{\theta}_t^{hist} \in \mathbb{N}^{180}$
15: **end for**
16: $\boldsymbol{c}_t^{sort} \in \mathbb{N}^{121} \leftarrow \mathrm{Sort}((\boldsymbol{\theta}_t^{hist})_{29:149})$
17: $\boldsymbol{\theta}_t^{sort} \in \mathbb{N}^{121} \leftarrow \mathrm{argSort}((\boldsymbol{\theta}_t^{hist})_{29:149})$
18: $\boldsymbol{c}_t^{best3} \in \mathbb{R}^3 \leftarrow (\boldsymbol{c}_t^{sort})_{119:121} / \sum_{i=119}^{121}(\boldsymbol{c}_t^{sort})_i$
19: $\boldsymbol{\theta}_t^{best3} \in \mathbb{N}^3 \leftarrow (\boldsymbol{\theta}_t^{sort})_{119:121}$
20: $\theta_t^{vv} \leftarrow \boldsymbol{\theta}_t^{best3} \cdot \boldsymbol{c}_t^{best3} + 30$
21: $$\theta_t^{vv} \leftarrow \begin{cases} K_1^\theta\ \theta_t^{vv} + (1 - K_1^\theta)\ \theta_{t-1}^{vv} & (|\theta_t^{vv} - \theta_{t-1}^{vv}| \le 4°) \\ K_2^\theta\ \theta_t^{vv} + (1 - K_2^\theta))\ \theta_{t-1}^{vv} & (|\theta_t^{vv} - \theta_{t-1}^{vv}| > 4°) \end{cases}$$
22: $$\boldsymbol{vv}_t = \begin{bmatrix} vv_t^x \\ vv_t^y \\ vv_t^z \end{bmatrix} \leftarrow \begin{bmatrix} 9.81\ \cos(\theta_t^{vv}\ \pi/180) \\ 9.81\ \sin(\theta_t^{vv}\ \pi/180) \\ 0 \end{bmatrix}$$
23: $\boldsymbol{vv}(t) \leftarrow \mathrm{ZOH}(\boldsymbol{vv}_t)$

magnitudes M_t and angles Θ_t can be calculated from $\nabla \boldsymbol{x}_t$ and $\nabla \boldsymbol{y}_t$ in steps 5-6 of Algorithm 1. Here, $\odot$ and $\oslash$ are Hadamard products and divisions that are element-wise products and divisions.

In Θ_t, we equate [360°, 180°] to [0°, 179°], because the angle of a person's neck usually does not exceed 180° (Algorithm 1, steps 8-11). Further, as the magnitude of the gradient is larger, the edge becomes more likely (see Fig. 2 (b)). The gradient magnitudes $\boldsymbol{M}_t$ are normalized through the global maximum and minimum to $[0, 1]$ (Algorithm 1, step 12).

Next, as shown in Fig. 2 (c), the histogram of gradient angles is calculated using an indicator function from Θ_t with its weight matrix $\boldsymbol{M}_t$ (Algorithm 1, steps 13-15). The number of bins in the histogram is set to 180. After calculating the histogram, the gradient's angles in the range [30°, 150°] are sorted in ascending order by their counts (Algorithm 1, steps 16-17). We assume that the passenger head will not rotate out of the range [30°, 150°] in most driving situations.

Subsequently, the best three angles $\boldsymbol{\theta}_t^{best3}$ are selected based on the highest three counts $\boldsymbol{c}_t^{best3}$ (Algorithm 1, steps 18-19).

Then, the direction of the visual vertical θ_t^{vv} is calculated as Step 20 of Algorithm 1, in which $\boldsymbol{c}_t^{best3}$ can be considered as the weight of $\boldsymbol{\theta}_t^{best3}$.

Meanwhile, the direction of the visual vertical θ_t^{vv} is also affected by the direction of the visual vertical in the previous frame, that is, θ_{t-1}^{vv}. As shown in Step 21 of Algorithm 1, we choose two different strategies to update θ_t^{vv} to reduce the instability due to the prediction errors with $K_1^{\theta} = 0.7$ and $K_2^{\theta} = 0.2$ empirically set in this study. An example to show the visualization of θ_t^{vv} in Fig. 2 (d) and (e).

In Step 23 of Algorithm 1, the visual vertical vector $\boldsymbol{vv} = [vv_x, vv_y, vv_z]^T$ is calculated from θ_t^{vv} with a fixed L2 norm 9.81 m/s^2. Notably, the value on the z-axis of $\boldsymbol{vv}$, i. e., vv_z, should be 0 because θ^{vv} is the rotation angle on the x-y plane of the head coordinate system.

In Step 24 of Algorithm 1, as the 6 DoF SVC model is a continuous-time system, $\boldsymbol{vv}_t$ is a discrete variable estimated from an image, a zero-order holder (ZOH) is used to convert $\boldsymbol{vv}_t$ into a continuous variable $\boldsymbol{vv}(t)$.

After block VVP, block $\boxed{\mathbf{VIS}_g}$ transfers $\boldsymbol{vv}$ to the sensed visual vertical $\boldsymbol{vv}_s$. Note that the vertical signals $\boldsymbol{vv}_s$ and $\boldsymbol{v}_s$ sensed by the visual and vestibular systems are assumed to be 3D. For simplicity, a 3×3 identity matrix $\boldsymbol{I}_{3\times3}$ is used as the transform matrix in this study. Thus,

$$\boldsymbol{vv}_s = \boldsymbol{I}_{3\times3}\ \boldsymbol{vv} = \begin{bmatrix} 1 & 0 & 0 \\ 0 & 1 & 0 \\ 0 & 0 & 1 \end{bmatrix} \begin{bmatrix} vv_x \\ vv_y \\ vv_z \end{bmatrix}. \tag{1}$$

B. Vestibular System Modeling

The vestibular system is mainly composed of otolith organs and semi-circular canals. As shown in Fig. 1, the otolith organ is modeled as a **OTO** block. Its input is the gravity-inertial acceleration (GIA) in 3 DoF, which is $\boldsymbol{f = a + g}$. Here, $\boldsymbol{a}$ is the inertial acceleration, and $\boldsymbol{g}$ is the gravitational acceleration (upward). Refer to [23], in the **OTO** block, a 3×3 identity matrix $\boldsymbol{I}_{3\times3}$ is used for transforming $\boldsymbol{f}$ to the sensed GIA $\boldsymbol{f}_s$ as $\boldsymbol{f}_s = \boldsymbol{I}_{3\times3}\ \boldsymbol{f}$.

Further, the **SCC** block contained semi-circular canals. It receives angular velocity $\boldsymbol{\omega}$ in 3 DoF and transforms it into the sensed angular velocity $\boldsymbol{\omega}_s$ using a transfer function [32]:

$$\boldsymbol{\omega}_s = \frac{\tau_a \tau_d s^2}{(\tau_a s + 1)(\tau_d s + 1)}\boldsymbol{\omega}. \tag{2}$$

Subsequently, block **LP** represents the otolith-canal interaction that estimates the detected vertical signal $\boldsymbol{v}_s$ from $\boldsymbol{f}_s$ and $\boldsymbol{\omega}_s$ by updating the raw [33]:

$$\frac{d\boldsymbol{v}_s}{dt} = \frac{1}{\tau}(\boldsymbol{f}_s - \boldsymbol{v}_s) - \boldsymbol{\omega}_s \times \boldsymbol{v}_s. \tag{3}$$

Moreover, the sensed inertial acceleration $\boldsymbol{a}_s$ can be calculated as $\boldsymbol{a}_s = \boldsymbol{f}_s - \boldsymbol{v}_s$.

C. Internal Models

The internal model is a hypothetical central neural representation of anticipatory information generated by the central nervous system concerning the sensory organs. As shown in Fig. 1, the 6 DoF SVC-VV model has three internal models. Specifically, the internal models of **SCC**, **OTO**, and $\boxed{\mathbf{VIS}_g}$ are modeled as blocks of $\overline{\mathbf{SCC}}$, $\overline{\mathbf{OTO}}$, and $\overline{\mathbf{VIS_g}}$, respectively. Furthermore, the low-pass filter in the vestibular system, which separates the perceived signals of vertical and linear acceleration, is also modeled as $\overline{\mathbf{LP}}$ in the internal model.

For blocks $\overline{\mathbf{SCC}}$ and $\overline{\mathbf{OTO}}$, there are two types of inputs. One type includes a variety of signals to help create motion perceptions, such as motion predictions [34] and efference copy [35], which is an internal copy of the neural signal that generates the movement. The other types are obtained from the feedback of conflicts between the sensor organs and their internal model.

The $\overline{\mathbf{SCC}}$ represents the internal model of SCC, which transforms angular velocity $\hat{\boldsymbol{\omega}}$ predicted through the internal model to the sensed angular velocity $\hat{\boldsymbol{\omega}}_s$ using a transfer function [32]:

$$\hat{\boldsymbol{\omega}}_s = \frac{\tau_d s}{\tau_d s + 1}\hat{\boldsymbol{\omega}}. \tag{4}$$

The predicted $\hat{\boldsymbol{\omega}}$ combines the angular velocity signal $\tilde{\boldsymbol{\omega}}$ and the feedback of the difference $\Delta\boldsymbol{\omega}$ between sensory information $\boldsymbol{\omega}_s$ and estimated information $\hat{\boldsymbol{\omega}}_s$, that is, $\Delta\boldsymbol{\omega} = \boldsymbol{\omega}_s - \hat{\boldsymbol{\omega}}_s$. To simplify the generation process of a variety of signals to help create motion perceptions, this study uses the angular velocity of the head $\boldsymbol{\omega}$ as input. Therefore,

$$\begin{aligned} \hat{\boldsymbol{\omega}} &= \tilde{\boldsymbol{\omega}} + K_{\omega c}\Delta\boldsymbol{\omega} \\ &= K_{\omega}\boldsymbol{\omega} + K_{\omega c}(\boldsymbol{\omega}_s - \hat{\boldsymbol{\omega}}_s). \end{aligned} \tag{5}$$

The $\overline{\mathbf{OTO}}$ represents the internal model of OTO, which transforms predicted GIA $\hat{\boldsymbol{f}}$ into the expected afferent signal of GIA $\hat{\boldsymbol{f}}_s$ using a 3×3 identity matrix $\boldsymbol{I}_{3\times3}$, that is $\hat{\boldsymbol{f}}_s = \boldsymbol{I}_{3\times3}\ \hat{\boldsymbol{f}}$. The predicted $\hat{\boldsymbol{f}}$ can be calculated as follows:

$$\hat{\boldsymbol{f}} = \hat{\boldsymbol{g}} + \hat{\boldsymbol{a}}, \tag{6}$$

where $\hat{\boldsymbol{a}}$ and $\hat{\boldsymbol{g}}$ are the gravitational and linear accelerations predicted by the internal model. Specifically,

$$\begin{aligned} \hat{\boldsymbol{a}} &= \tilde{\boldsymbol{a}} + K_{ac}\Delta\boldsymbol{a} \\ &= K_a\boldsymbol{a} + K_{ac}(\boldsymbol{a}_s - \hat{\boldsymbol{a}}_s); \end{aligned} \tag{7}$$

In part, the acceleration $\boldsymbol{a}$ is calculated from measured GIA $\boldsymbol{f}$, that is, $\boldsymbol{a} = \boldsymbol{f} - \boldsymbol{g}$. According to [23], gravitational acceleration $\boldsymbol{g}$ is calculated from $\boldsymbol{\omega}_q$ using the following update law:

$$\frac{d\boldsymbol{g}}{dt} = -\boldsymbol{\omega} \times \boldsymbol{g}. \tag{8}$$

However, in practice, noise exists in $\boldsymbol{\omega}$ obtained from the IMU. This results in a drift in $\boldsymbol{g}$ because the noise in $\boldsymbol{\omega}$ is also integrated. To solve this problem, $\boldsymbol{\omega}_q$ is a calibrated angle velocity obtained using a complementary filter [36] to reduce the sensing tilt from the IMU. Complementary filter $Q(\boldsymbol{\omega}, \boldsymbol{f})$ outputs a quaternion vector $\boldsymbol{q} \in \mathbb{R}^4$ to present the orientation calculated from the $\boldsymbol{\omega}$ and $\boldsymbol{f}$:

$$\boldsymbol{q} = Q(\boldsymbol{\omega}, \boldsymbol{f}). \tag{9}$$

Then, $\boldsymbol{\omega_q}$ can be approximated as

$$\boldsymbol{\omega_q} = \begin{bmatrix} 0 & 1 & 0 & 0 \\ 0 & 0 & 1 & q0 \\ 0 & 0 & 0 & 1 \end{bmatrix} (2\frac{d\boldsymbol{q}}{dt} \circ \boldsymbol{q}^{-1}), \tag{10}$$

where $\circ$ denotes the quaternion product. Thus, the new update law for $\boldsymbol{g}$ is

$$\frac{d\boldsymbol{g}}{dt} = -\boldsymbol{\omega_q} \times \boldsymbol{g}. \tag{11}$$

Then, $\boldsymbol{g}$ is normalized in a fixed L2 norm 9.81 m/s^2 by

$$\boldsymbol{g} = 9.81 \ \frac{\boldsymbol{g}}{||\boldsymbol{g}||}. \tag{12}$$

In addition, the $\hat{\boldsymbol{g}}$ in part of $\hat{\boldsymbol{f}} = \hat{\boldsymbol{g}} + \hat{\boldsymbol{a}}$ (i.e., Eq. 6) is calculated via

$$\begin{aligned} \hat{\boldsymbol{g}} &= \boldsymbol{K}_{vvc} \int_0^t \Delta\boldsymbol{v}\boldsymbol{v} dt + \boldsymbol{K}_{vc} \int_0^t \Delta\boldsymbol{v} dt \\ &= \boldsymbol{K}_{vvc} \int_0^t (\boldsymbol{v}\boldsymbol{v}_s - \hat{\boldsymbol{v}}\hat{\boldsymbol{v}}_s) dt \\ &\quad + \boldsymbol{K}_{vc} \int_0^t (\boldsymbol{v}_s - \hat{\boldsymbol{v}}_s) dt. \end{aligned} \tag{13}$$

Here, $\Delta\boldsymbol{v}$ and $\Delta\boldsymbol{v}\boldsymbol{v}$ are the conflicts of the vertical and visual vertical signals between the sensor organs and their internal model, respectively. The $\hat{\boldsymbol{v}}_s$ is calculated by $\boxed{\overline{\mathbf{LP}}}$ block by following update law [33]:

$$\frac{d\hat{\boldsymbol{v}}_s}{dt} = \frac{1}{\tau}(\hat{\boldsymbol{f}}_s - \hat{\boldsymbol{v}}_s) - \hat{\boldsymbol{\omega}}_s \times \hat{\boldsymbol{v}}_s, \tag{14}$$

which is the same as the update law for $\boldsymbol{v}_s$. Subsequently, $\hat{\boldsymbol{a}}_s$ in Eq. 7 is calculated using $\hat{\boldsymbol{a}}_s = \hat{\boldsymbol{f}}_s - \hat{\boldsymbol{v}}_s$.

Meanwhile, $\hat{\boldsymbol{v}}\hat{\boldsymbol{v}}_s$ represents the sensed visual vertical in the internal model, which is calculated by block $\boxed{\overline{\mathbf{VIS_g}}}$ using the vertical sensed although visual-vestibular interaction, that is, $\hat{\boldsymbol{g}}$. Thus,

$$\hat{\boldsymbol{v}}\hat{\boldsymbol{v}}_s = \boldsymbol{T}_{\overline{vis}}\ \hat{\boldsymbol{g}} = \begin{bmatrix} 1 & 0 & 0 \\ 0 & 1 & 0 \\ 0 & 0 & 0 \end{bmatrix} \begin{bmatrix} \hat{g}_x \\ \hat{g}_y \\ \hat{g}_z \end{bmatrix}, \tag{15}$$

that projects the sensed vertical $\hat{\boldsymbol{g}}$ into the x-y plane in the head coordinate system, eliminating the value on the z-axis. Finally, $\hat{\boldsymbol{g}}$ can be updated by

$$\frac{d\hat{\boldsymbol{g}}}{dt} = \boldsymbol{K}_{vvc}\ (\boldsymbol{v}\boldsymbol{v}_s - \hat{\boldsymbol{v}}\hat{\boldsymbol{v}}_s) + \boldsymbol{K}_{vc}(\boldsymbol{v}_s - \hat{\boldsymbol{v}}_s). \tag{16}$$

D. Motion Sickness Estimation

According to the SVC theory [21], motion sickness is mainly caused by a conflict between vertical perception through sensory organs and vertical feeling estimated by their internal models. Therefore, [22] proposed that motion sickness incidence (MSI), which represents the percentage of vomiting subjects, is determined by the conflict of vertical signals $\Delta\boldsymbol{v} = \boldsymbol{v}_s - \hat{\boldsymbol{v}}_s$ using

$$MSI = \frac{P}{(\tau_l s + 1)^2}\ H, \tag{17}$$

where P is a parameter and

$$H = \frac{||\Delta\boldsymbol{v}||/b}{1 + ||\Delta\boldsymbol{v}||/b} \tag{18}$$

is the Hill function that normalizes the L2 norm of the vertical conflict signal $||\Delta\boldsymbol{v}||$ to [0,1) and b is its parameter.

III. Simulation Experiment

To confirm the effects of incorporating visual vertical into the 6 DoF SVC model on prediction accuracy, we initially compared the predicted MSI to the MSI observed in McCauley et al.'s experiment [37]. In the experiment, the number of participants who vomited during two hours of exposure to 25 vertical motion profiles with various combinations of accelerations and frequencies was measured and MSI was calculated.

In our numerical simulation experiments, we predicted the MSI for a total of 50 motion profiles, including these 25 motion profiles. More specifically, based on the head coordinate system depicted in Fig. 8, we set

$$\begin{aligned} a_x(t) &= 0\ [m/s^2], \\ a_y(t) &= 9.81\ \sqrt{2}\ rms_i\ \ \sin(2\pi\ \ freq_i\ t)\ [m/s^2], \\ a_z(t) &= 0\ [m/s^2], \end{aligned}$$

where, $t \in \{0 : 7200\}$ $[s]$, $dt = 0.01$ $[s]$. Here, $freq_i \in \{0.083, 0.167, 0.180, 0.200, 0.250, 0.333, 0.417, 0.500, 0.600, 0.700\}$ $[Hz]$ and $rms_j \in \{0.0278, 0.055, 0.111, 0.170, 0.222, 0.234, 0.333, 0.444, 0.555\}$ $[g]$. We also made the assumption that $\boldsymbol{v}\boldsymbol{v} = \boldsymbol{g} = [0, 9.81, 0]$ $[m/s^2]$.

As shown in Table I, a conventional 6 DoF SVC model proposed by [24] (called the In1 model in this study) and its optimized parameters were used as a baseline. Furthermore, two sets of parameters were prepared for the 6 DoF SVC-VV model which were the same as those of the 6 DoF SVC model, i.e., In1 model in [24], except for K_{vc} and a new parameter K_{vvc}. Specifically, for the 6 DoF SVC-VV model (I), we employed $K_{vc} = 5.0$ and $K_{vvc} = 5.0$ to balance the feedback strength of the two conflict signals. Moreover, for the 6 DoF SVC-VV model (II), the parameters $K_{vvc} = 2.5$ $K_{vc} = 2.5$ were used to mitigate the excessive influence of those vertical confusion feedbacks on $\hat{\boldsymbol{f}}$.

The comparisons of the MSIs predicted by the three models shown in Table I and the MSIs measured in [37] are shown in Fig. 3. In Figs. 3(a), 3(b) and 3(c), the MSI predicted by the model is represented by the surface plots, while the black data points represent the MSI observed in [37].

To evaluate the difference between the predicted MSI and the ground truth of MSI, i.e., the measured MSI, under the 25 motion profiles, the mean square error (MSE) between them was calculated. Figure. 3(d) shows that the MSE for both the 6 DoF SVC model and 6 DoF SVC-VV model (I) model were approximately around 6%, while that for the 6 DoF SVC-VV model (II) was approximately 10%. In addition,the peak of MSI predicted by the 6 DoF SVC-VV model (II) shifts to a lower frequency, i.e., 0.167 $[Hz]$.

TABLE I
PARAMETERS FOR THE 6 DOF SVC MODEL AND THE 6 DOF SVC-VV MODELS

Models	K_a	K_ω	$K_{\omega c}$	K_{ac}	K_{vc}	K_{vvc}	τ $[s]$	τ_a $[s]$	τ_d $[s]$	b $[m/s^2]$	τ_I $[s]$	P $[\%]$
6 DoF SVC (In1) [24]	0.1	0.1	10	0.5	**5.0**	**n/a**	2.0	190.0	7.0	0.5	720.0	85
6 DoF SVC-VV (I)	0.1	0.1	10	0.5	**5.0**	**5.0**	2.0	190.0	7.0	0.5	720.0	85
6 DoF SVC-VV (II)	0.1	0.1	10	0.5	**2.5**	**2.5**	2.0	190.0	7.0	0.5	720.0	85

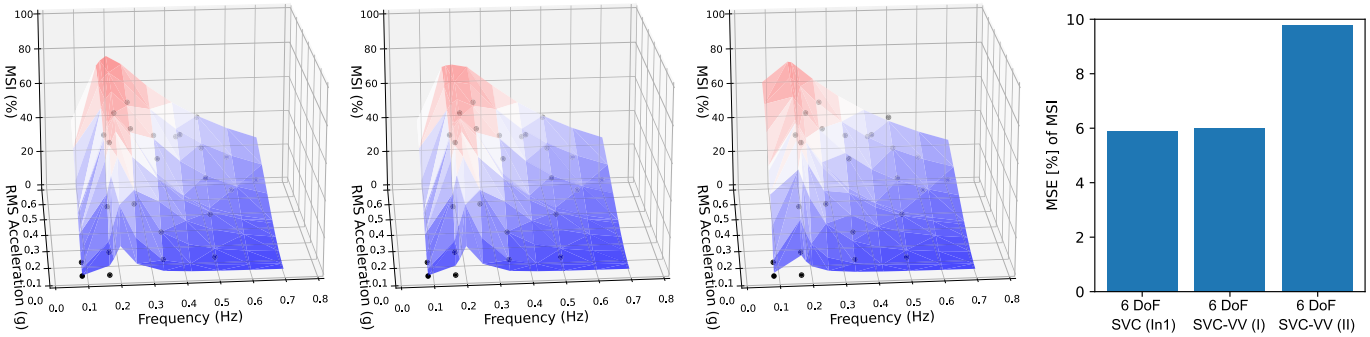

(a) Predicted MSIs by 6 DoF SVC (In1) model [24]
(b) Predicted MSIs by 6 DoF SVC-VV model (I)
(c) Predicted MSIs by 6 DoF SVC-VV model (II)
(d) MSE between predicted MSIs and observed MSIs in [37]

Fig. 3. Comparison of the predicted MSIs from the three models, as indicated in Table I, with the MSIs measured in [37]. In Figures (a), (b) and (c), the black data points represent the actual MSI measured by [37].

Consequently, for the driving experiment detailed in the next section, the parameters of 6 DoF SVC-VV model (I) were used.

IV. DRIVING EXPERIMENT

This experiment aimed to verify whether the proposed 6 DoF SVC-VV model can predict MSI while riding an APMV with different visual conditions. Therefore, two APMV ride comparison conditions were established for this experiment: 1) looking ahead during autonomous driving (LAD), and 2) working with a tablet device during autonomous driving (WAD). Considering that the tablet device used in WAD may hinder passengers' visual-spatial perception, we propose the following hypothesis:

H: Passengers working while riding the APMV will have a higher probability of getting motion sickness than if they look ahead while riding the APMV.

To simulate the use of APMV in stations or shopping malls where frequent pedestrian avoidance is required, an experiment in which participants rode an APMV was conducted in an indoor room environment. This study was carried out with the approval of the Research Ethics Committee of Nara Institute of Science and Technology (No. 2021-I-38).

A. Autonomous Personal Mobility Vehicle

In this experiment, a robotic wheelchair *WHILL Model CR* with an autonomous driving system was used as the APMV. As shown in Fig. 4, the APMV was equipped with multilayered LiDAR (Velodyne VLP-16) and a controlling laptop PC. An autonomous driving system based on the *Robot Operating System* was applied to the APMV. LiDAR was utilized for self-localization by the *adaptive Monte Carlo localization* method on a previously built environmental map using the *simultaneous localization and mapping* method.

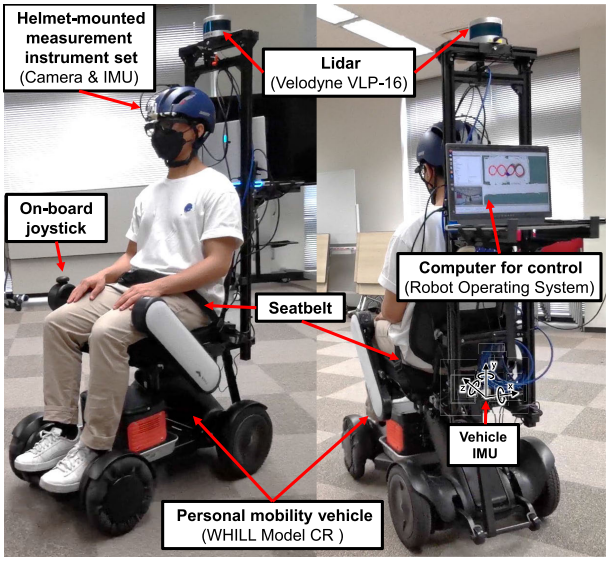

Fig. 4. Autonomous driving robotic wheelchair used as the experimental vehicle.

Thus, it could automatically drive on pre-designed routes using a path-following controller [38].

To ensure the experiment safety, the APMV had an automatic brake function that was applied when there was an obstacle within 0.5 meters directly in front of it. Passengers could also actively control the APMV with the on-board joystick and power button if they feel in danger. Meanwhile, a wireless remote controller could control the APMV to stop based on the actual risks during the experiment. Further, the maximum velocity was set to 6 $[km/h]$, and the maximum linear acceleration was set to 1.7 $[m/s^2]$.

B. Driving Conditions

As shown in Fig. 5, a 6 $[m]\times 12.5$ $[m]$ room at Nara Institute of Science and Technology was used as the experimental site.

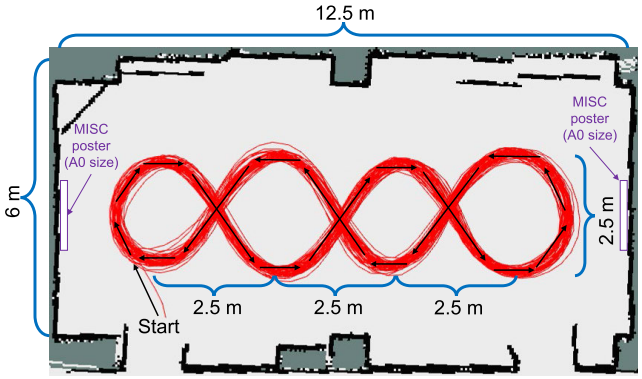

Fig. 5. A 12.5 $[m] \times 6$ $[m]$ room used as the experimental environment. A slalom path was used for autonomous driving. Two MISC posters (see Fig. 9) were mounted on the walls at either end of the room.

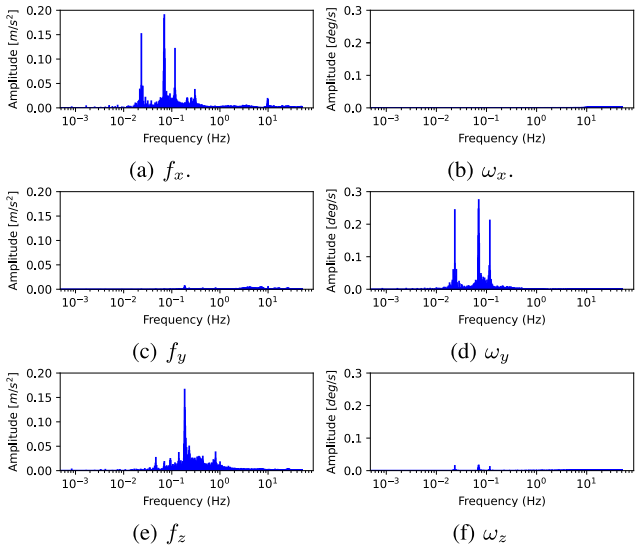

Fig. 6. Amplitude (scaled by 2/N) and frequency of linear acceleration ($\boldsymbol{f}$) and angle velocity ($\boldsymbol{\omega}$) measured from a IMU on the AMPV. Here, its coordinate system is parallel to the head coordinate system shown in Fig. 4.

The target temperature of the air conditioner in the room was set as 25°C. In this experiment, a 20 minutes slalom driving path (see the red line in Fig. 5) was designed to simulate APMV avoiding other traffic participants in mixed traffic, such as shared space. Specifically, APMV performed slalom driving with four centers of rotation such that the number of left and right rotations was the same. The diameter of each rotation was approximately 2.5 $[m]$; therefore, the distance between the two rotary centers was also 2.5 $[m]$. The amplitude and frequency of linear acceleration ($\boldsymbol{f}$) and angle velocity ($\boldsymbol{\omega}$) measured from an IMU on the AMPV during 20 minutes of slalom driving are shown in Fig. 6. The coordinate system of the vehicle IMU is shown in Fig. 4.

In addition, to reduce the effect of the participants' predictions of driving dynamics on their motion sickness, no actual object was placed in these centers of rotation.

C. Riding Conditions

As shown in Fig. 7, two riding conditions were designed: 1) looking ahead during autonomous driving (LAD) and 2) working with a tablet device during autonomous driving (WAD). Each scenario took 25 minutes, including 20 minutes

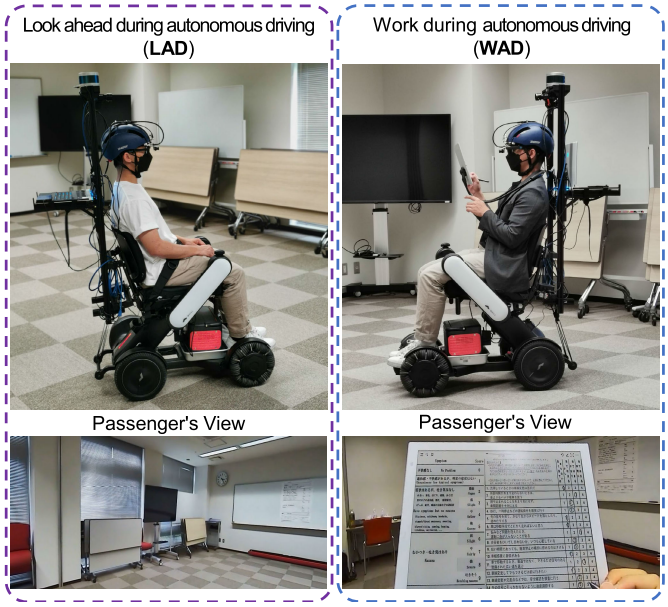

Fig. 7. Two riding conditions: 1) looking ahead during autonomous driving (LAD); 2) working with a tablet device during autonomous driving (WAD).

of autonomous driving and 5 minutes of parking. The detailed design of each scenario is as follows.

1) Looking Ahead During Autonomous Driving (LAD): In the LAD, participants were asked to look ahead during 20 minutes of autonomous driving and 5 minutes of parking. It was also hypothesized that participants could easily obtain vertical orientation information from the floor, walls, and surrounding objects such as windows, tables, chairs, and whiteboards.

2) Working With a Tablet Device During Autonomous Driving (WAD): In the WAD, participants were asked to work with a tablet device (Sony DPT-RP1 Digital Paper: 224 [mm] high with 302.6 [mm] weight for horizontal use). They were asked to use a stylus to answer dummy questionnaires and read articles on e-books during 20 minutes of autonomous driving and 5 minutes of parking. Note that the contents of these questionnaires and articles were not relevant to this experiment to avoid influencing the experimental results. Moreover, a neck-hanging tablet stand was used to help participants hold the e-book, see the text clearly, and write more easily. It also enabled the relative positions of the head and tablet device to be maintained within a certain range.

This scenario was also hypothesized to be more prone to cause motion sickness because the participants may experience difficulty in recognizing the vertical direction because the tablet device prevented the passenger from perceiving the body motion from dynamic visual information [12] such as optical flow, and static visual information such as horizontal or vertical.

D. Measurements

1) Head Movement and Visual Information: To measure the acceleration and angular velocity of the passenger's head and visual information, a helmet-mounted measurement instrument (HMMI) was used (see Fig. 8). The HMMI included an inertial measurement unit(IMU) and a camera set in front of a

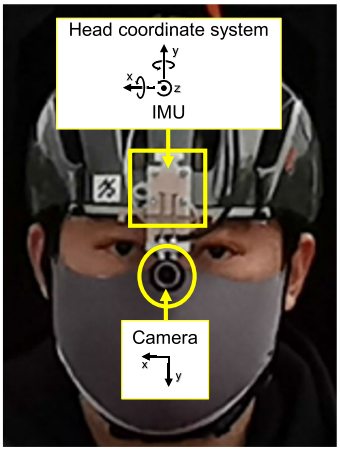

Fig. 8. A helmet-mounted measurement instrument (HMMI): an IMU and a camera were placed on a helmet to observe the acceleration and angular velocity of the passenger's head and visual information.

Symptom		Score
不快感なし No Problem		0
違和感・不快感があるが、特定の症状はない Uneasiness (no typical symptoms)		1
症状はあるが，吐き気はなし めまい，寒気，ほてり，頭痛，あくび， 胃やのどの違和感，発汗， 眼精疲労， げっぷ，疲労，唾液の分泌などの諸症状 Have symptoms but no nausea Dizziness, cold/warm, headache, stomach/throat awareness, sweating, blurred vision, yawning, burping, tiredness, salivation, ...	微弱 Vague	2
	弱 Slight	3
	中 Rather	4
	強 Severe	5
むかつき・吐き気はあり Nausea	弱 Slight	6
	中 Fairly	7
	強 Severe	8
	吐きそう Retching nausea	9
嘔吐 Vomiting		10

Fig. 9. An 11-point MIsery SCale (MISC) [39] in japanese and english.

helmet. The IMU measured 3 DoF acceleration f and 3 DoF angular velocity ω at 100 [Hz]. The camera resolution was set to 1280 × 720 pixels at 30 [Hz]. To reduce the impact of lens distortion on the visual vertical prediction, we cropped the periphery of the camera video. The cropped resolution was 1000 × 480.

2) Motion Sickness: To measure the severity of motion sickness during the 25 minutes experiment, participants verbally reported their feelings of motion sickness every minute using an 11-point MIsery SCale (MISC) [39] ranging from zero to 10 (see Fig. 9). If MISC reached 6 and lasted for more than 2 minutes, then the APMV stopped, and participants continued to sit on the stopped APMV to report MISC every minute for 5 min. To help participants refer to the definition of MISC, the two A0 size posters in Fig. 9 were placed on whiteboards on both sides of the room in the LAD scenario; and the definition of MISC was available on each page of the e-book in the WAD scenario (see Fig. 7).

E. Participants and Groups

A total of 27 participants (10 females and 17 males) participated in this experiment as users of APMV. They were 22-29 years old (mean:23.5, standard deviation,1.89). They had no experience with autonomous cars and APMVs before this experiment. All participants provided informed consent before participating in the experiment. Each participant was asked to ride the APMV under the LAD and WAD conditions once. To avoid the order effect of the experimental conditions on the experimental results, participants were randomly assigned to two groups. Specifically, 14 participants in a group called *LAD→WAD* experienced the LAD scenario first and then the WAD scenario. Thirteen participants in another group called *WAD→LAD* experienced these conditions in the opposite order.

The minimum time interval between the two conditions was 24 hours. The total time of this experiment, including the two conditions was four hours for each participant. Each participant received 4,000 Japanese Yen as a reward.

F. Procedure

First, the participants were instructed by following information before the experiment:

- The purpose of the experiment was to investigate the effect of the riding conditions of an APMV on motion sickness.
- In this experiment, participants rode on the APMV and experienced slalom driving repeatedly (up to 6 km/h).
- There were two riding conditions. Each riding scenario was performed on a separate day. Each scenario took approximately 2 hours, and the total time for the two conditions was approximately 4 hours.
- Details of those two riding conditions were introduced just before participants experienced one of them, separately.
- In each riding scenario, the APMV was autonomously driven in 20 minutes, then the APMV stopped, and participants could rest for 5 minutes on it.
- In those 25 minutes, participants were required to report a level of MISC in each minute based on their feelings of motion sickness.
- If the MISC reached 6 and lasted for more than 2 minutes, then the APMV was stopped immediately and participants continued to sit on the stopped APMV to report MISC every minute for 5 minutes.

Moreover, to reduce the restlessness and nervousness of the participants owing to lack of knowledge about APMV, we explained the principles of the autonomous driving system and its sensors (i. e., Lider), and the operational design domain (e. g., sensor range, maximum speed, maximum linear acceleration, and the judgment distance of emergency stop) to the participants in detail. Participants were allowed to actively take over and stop the APMV if they thought there was danger.

G. Motion Sickness Symptoms Reported by MISC

The MISC was reported by each participant every minute during each 25 minutes trial. For each participant, the mean of

TABLE II
DEFINITION OF CONFUSION MATRIX FOR EVALUATING MOTION SICKNESS PREDICTION BY COMPARING THE PREDICTED MSI TO THE REPORTED MISC

		MSI (Predicted result)	
		Positive ($MSI_{LAD} < MSI_{WAD}$)	Negative ($MSI_{LAD} \geq MSI_{WAD}$)
MISC (True result)	Positive ($MISC_{LAD} < MISC_{WAD}$)	TP (True Positive)	FN (False Negative)
	Negative ($MISC_{LAD} \geq MISC_{WAD}$)	FP (False Positive)	TN (True Negative)

TABLE III
EVALUATION INDEXES FOR THE PREDICTION OF MOTION SICKNESS USING PREDICTED MSI COMPARED TO REPORTED MISC

Evaluation index	Explanation
$Accuracy = \frac{TP+TN}{TP+TN+FP+FN}$	Rate of the correct predictions over all predictions.
$Precision = \frac{TP}{TP+FP}$	Rate of correct positive predictions over all positive predictions.
$Recall = \frac{TP}{TP+FN}$	Rate of correct positive predictions over all the positive true results.
$F1\ score = \frac{2 \cdot Precision \cdot Recall}{Precision + Recall}$	The harmonic mean of the precision and recall.

the MISC was calculated to evaluate the participant's susceptibility to motion sickness, while the maximum of the MISC was also calculated to evaluate the participant's progression of motion sickness.

We used 2×2 mixed-design ANOVAs to evaluate the mean and maximum of MISC in two riding conditions (within-subject factor: LAD and WAD) between two groups of condition order (between-subject factor: *LAD→WAD* and *WAD→LAD*). Further, MISC results were also analyzed under LAD and WAD conditions to test whether our proposed hypothesis $\boldsymbol{H}$, i. e., passengers working with a tablet device while riding the APMV will have a higher probability of getting motion sickness than if they look ahead while riding the APMV.

H. Calculated Visual Vertical

The calculated visual vertical of each trial was evaluated by analyzing the Pearson correlation coefficient between the direction of VV, i. e., θ^{vv}, and direction of gravitational acceleration, i. e., θ^{g}, from each 25 minutes trial independently. Particularly, θ^{vv} was estimated using Algorithm 1 from the camera data, and the direction of the gravitational acceleration projected in the 2D head coordinate system was calculated as $\theta^{g} = 180 \arctan(g_y/g_x)/\pi$. Here, the gravitational acceleration $\boldsymbol{g}$ was estimated from the IMU data, that is, $\boldsymbol{f}$ and $\boldsymbol{\omega}$. Moreover, a two-sided paired t-test was used to analyze the significant difference between the Pearson correlation coefficients for the LAD and WAD conditions.

I. Motion Sickness Prediction by MSI

The proposed 6 DoF SVC-VV model was used to predict the MSI from the IMU data (i. e., $\boldsymbol{f}$ and $\boldsymbol{\omega}$) and the camera images measured in the experiment. To implement the calculation of the zero-order holder, the calculated visual vertical was up-sampled from 30 [Hz] to 100 [Hz] by forward fill to synchronize with the IMU data.

To predict MSI, the parameters for the 6 DoF SVC model and the 6 DoF SVC-VV model used in this experiment are identical to those presented in Table I. It's important to note that the 6-DoF SVC-VV model employed the parameters of the 6-DoF SVC-VV model (I).

Similar to the MISC evaluation method, 2×2 mixed-design ANOVAs (within-subject factors: LAD and WAD; between-subject factors: *LAD→WAD* and *WAD→LAD*) were used to evaluate the mean and maximum values of the predicted MSI in LAD and WAD, respectively.

J. Comparison Between Predicted MSI and Reported MISC

To investigate the performance of the proposed 6 DoF SVC-VV model, we compared the predicted MSI with the reported MISC. Note that MSI and MISC are different indicators for each other. Basically, the MISC is an evaluation indicator for individuals, whereas the MSI is an evaluation indicator for the whole group, i. e., MSI indicates the percentage of participants who experienced vomiting when exposed to motion for a certain time, and MISC indicates the subjective assessment of each participant of the severity of motion sickness. Considering the difference in meaning between MSI and MISC, the performance of the proposed 6 DoF SVC-VV model was evaluated by comparing the high-low relationship of the reported MISC under the LAD and WAD, and that of the predicted MSI under those two riding conditions.

Based on the confusion matrix presented in Table II, multiple evaluation indexes, that is, accuracy, precision, recall, and F1 score (Table III), were used to evaluate the performance of the proposed 6 DoF SVC-VV model. We took each participant's reported MISC as the true result and the predicted

TABLE IV
TWO-WAY MIXED-DESIGN ANOVA FOR MEAN AND MAXIMUM OF MISC. * SHOWS THE $p < .05$

Measurement	Effect	SS	DF1	DF2	MS	*F-value*	*p-value*	η_p^2
Mean of MISC	Groups	0.092	1	25	0.092	0.065	0.801	0.003
	Conditions	2.506	1	25	2.506	4.296	**0.049** *	0.147
	Interaction	0.918	1	25	0.918	1.574	0.221	0.059
Maximum of MISC	Groups	0.002	1	25	0.002	0.000	0.986	0.000
	Conditions	6.685	1	25	6.685	3.362	0.079	0.119
	Interaction	1.101	1	25	1.101	0.553	0.464	0.022

MSI as the predicted result of their motion sickness. Therefore, as summarized in Table II, we refer to $\boldsymbol{H}$, $MISC_{LAD} < MISC_{WAD}$ and $MISC_{LAD} \geq MISC_{WAD}$ as the positive and negative states of the true result, respectively. Meanwhile, $MSI_{LAD} < MSI_{WAD}$ and $MSI_{LAD} \geq MSI_{WAD}$ are considered the positive and negative states of the predicted result, respectively. Moreover, the mean and maximum values were used as representative values for MISC and MSI.

V. RESULTS

A. Reported MISC

The MISC per minute reported for 27 participants is shown in Fig. 12. Among them, 21 participants reported that they developed symptoms of motion sickness in this experiment; however, six participants (four in group *LAD→WAD* and two in group *WAD→LAD*) reported $MISC = 0$ at all times in both the LAD and WAD conditions. In the WAD, participant #24 reported that $MISC = 6$ at approximately 8.5 minutes and was asked to stop the APMV. Then, the APMV was stopped, and the participant rested on the APMV. However, after 1 minut of rest, the motion sickness symptoms of participant #24 continued to develop to $MISC = 9$ at approximately 9.5 minutes, thus we immediately terminated the experiment.

For the two groups, i. e., *LAD→WAD* and *WAD→LAD*, we did not find a significant effect of the experimental order on the MISC results, as summarized in Table IV, and the mean and maximum of MISC during 25 minutes driving in LAD were lower than those in WAD, as shown in Fig. 10.

For two conditions, i. e., LAD and WAD, the two-way mixed-design ANOVA (see Table IV) reported that there was a significant difference in the mean MISC between conditions ($p = 0.049$); however, no significant difference between groups and in their interaction. Moreover, there was no significant difference in the maximum MISC between the groups, conditions, and their interactions.

B. Calculated Visual Vertical

Fig. 11 shows that θ^{vv} and θ^{g} had positive Pearson correlations ($N = 27, M = 0.27, SD = 0.12$) under the LAD condition, i. e., without the obstruction of view, and under the WAD condition ($N = 27, M = 0.20, SD = 0.17$), i. e., with obstruction of view. Furthermore, a two-sided paired t-test showed that the mean value of the Pearson correlation coefficients in the LAD condition was significantly higher than that in the WAD condition, i. e., $t(26) = 2.11$, $p = .044$, $cohen'd = 0.45$.

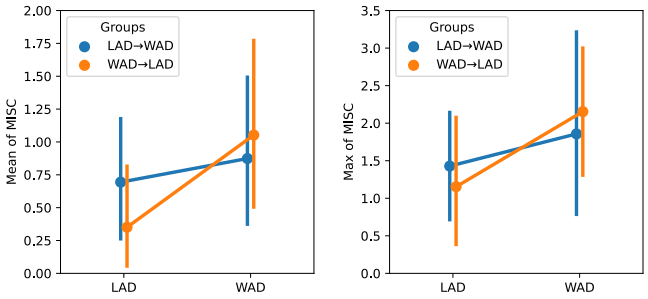

(a) Mean of MISC (b) Maximum of MISC

Fig. 10. Mean and maximum of MISC reported under LAD and WAD conditions (error bar: 95% confidence interval).

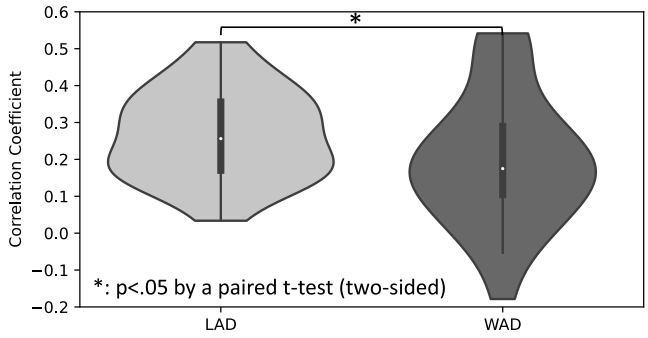

Fig. 11. Pearson correlation coefficients between the directions of the predicted visual vertical and estimated gravitational acceleration. A two-sided paired t-test reports their significant difference between LAD and WAD conditions.

C. Predicted MSI

The time series MSI predicted by the 6 DoF SVC and 6 DoF SVC-VV models are shown in Fig. 13. As a summarized index of the time-series MSI, the mean MSI predicted by the 6 DoF SVC and 6 DoF SVC-VV models are shown in Figs. 14-(a) and (b), respectively.

In Table V, a two-way mixed-design ANOVA for the mean MSI predicted by the 6 DoF SVC model revealed no significant effect of the groups, conditions, and in those interactions. The two-way mixed-design ANOVA for mean MSI predicted using the 6 DoF SVC-VV model revealed a significant main effect of conditions, with the LAD condition showing lower MSI than the WAD condition ($p = 0.008$); however, no significant effect was found in the groups and their interaction.

Using the maximum MSI as an evaluation index, Figs. 14 (c) and (d) show the maximum MSI predicted by the 6 DoF SVC and 6 DoF SVC-VV models, respectively. As presented in Table VI, a two-way mixed-design ANOVA

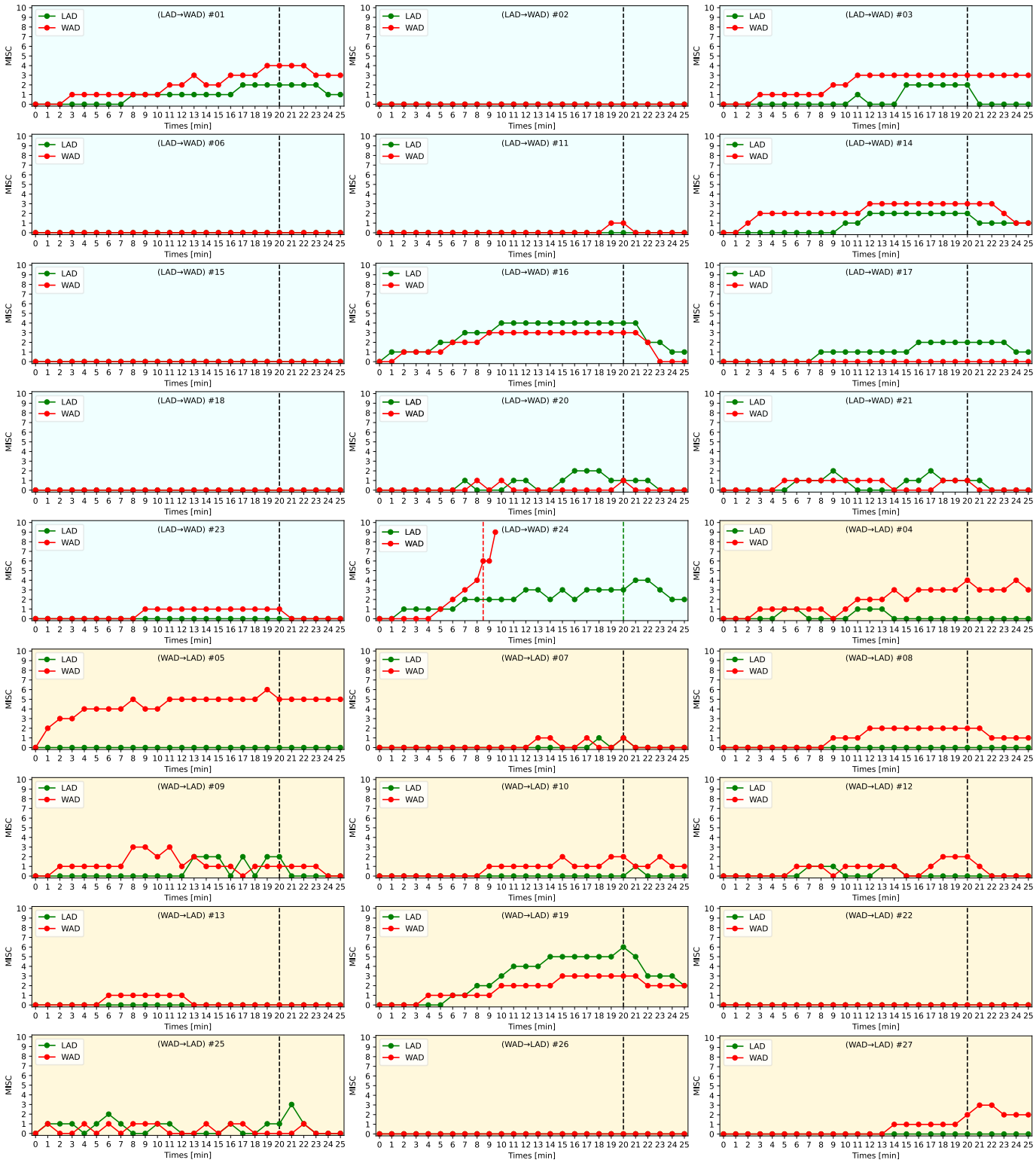

Fig. 12. MISC reported from 27 participants every minute. The horizontal coordinate shows the time whereas vertical coordinate shows the MISC. Graphs on the sky blue background represent MISCs reported by participants from *LAD→WAD* group whereas graphs on the yellow background represent MISCs reported by participants from *WAD→LAD* group. Green lines represent MISC reported by participants in LAD whereas red lines represent MISC reported by participants in WAD. The vertical broken lines indicate the moment of parking.

for the maximum MSI predicted by the 6 DoF SVC model revealed no significant effect of the groups, conditions, and interactions. For the maximum MSI predicted using the 6 DoF SVC-VV model, the two-way mixed-design ANOVA revealed a significant main effect of conditions, with the LAD condition showing significantly lower MSI than the WAD condition ($p = 0.004$); however, no significant effect was found in the groups and their interaction.

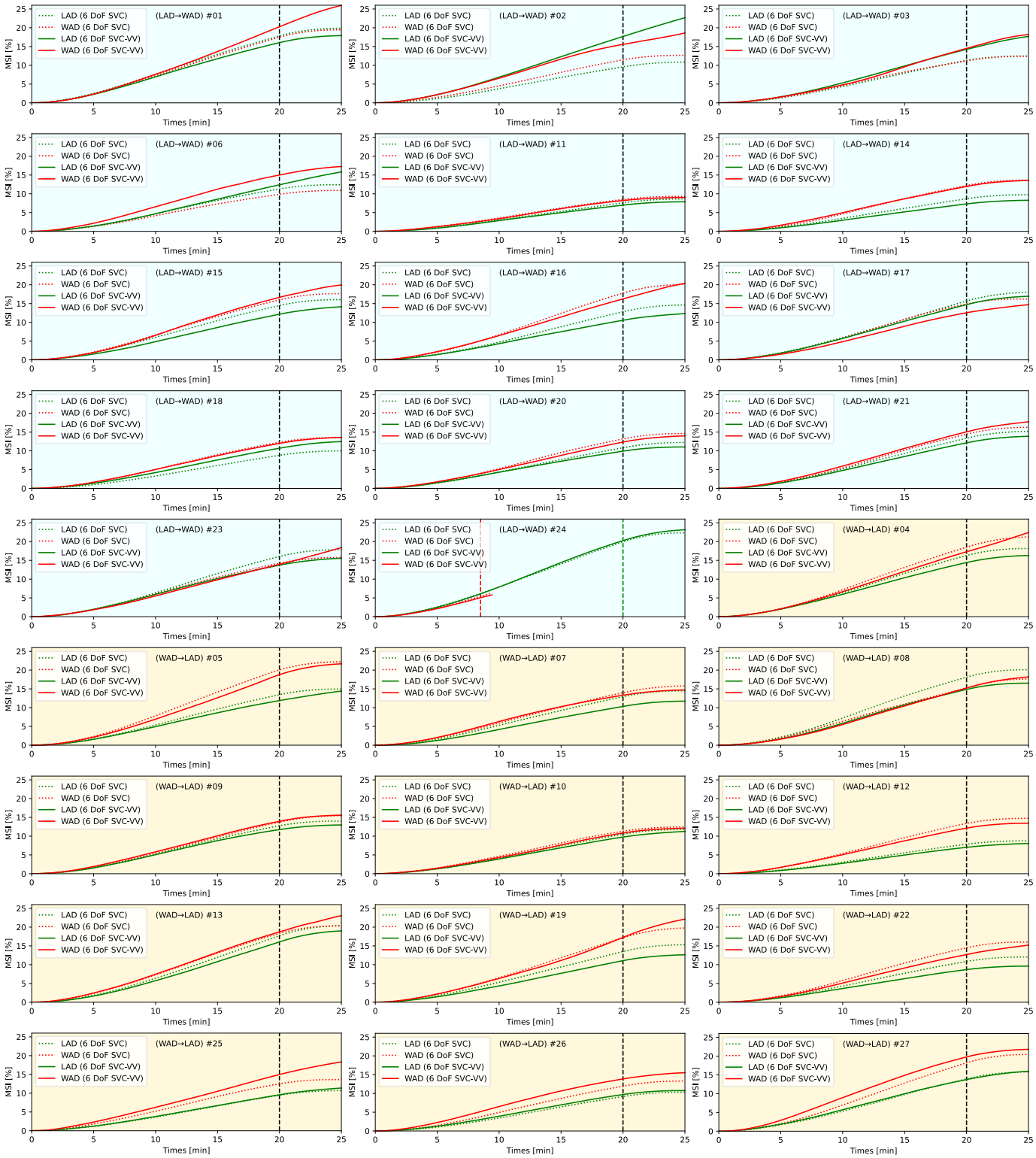

Fig. 13. Predicted MSI during the 25 minutes experiment by 6 DoF SVC and 6 DoF SVC-VV models for 27 participants. The horizontal coordinate is the time and the vertical coordinate is the vomiting rate, i. e., MSI. Graphs on the sky blue background represent MSIs predicted for participants from *LAD→WAD* group whereas graphs on the yellow background represent MSIs predicted for participants from *WAD→LAD* group. Green lines represent MISC reported by participants in LAD whereas red lines represent MISC reported by participants in WAD. Dotted lines represent MSI predicted by 6 DoF SVC model whereas solid lines represent MSI predicted by 6 DoF SVC-VV model. The vertical broken lines indicate the parking moment.

D. Comparison Between Predicted MSI and Reported MISC

As shown in Fig. 12, there were six participants (#02, #06, #15, #18, #22, #26) who did not get any motion sickness symptoms, i. e., all MISC reported were zero, in both LAD and WAD conditions. Considering that our proposed 6 DoF SVC-VV model was used to predict MSI, i. e., the percentage of participants who may vomit during the experiment, the

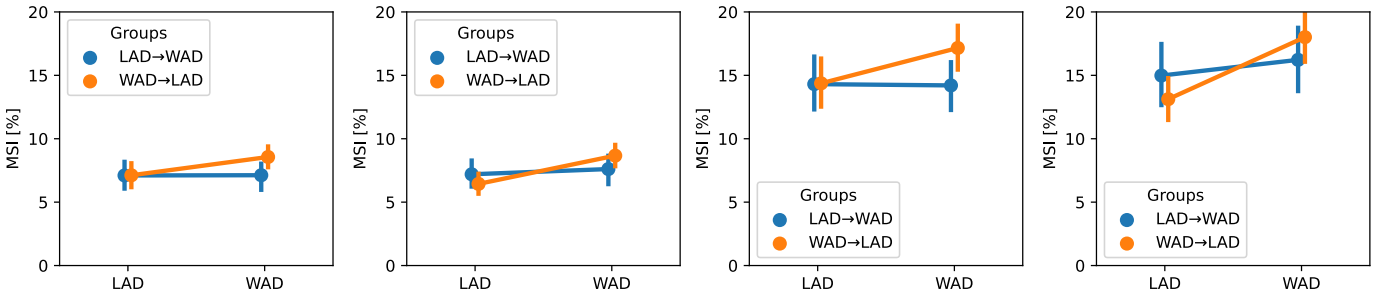

(a) Mean of MSI by 6 DoF SVC model
(b) Mean of MSI by 6 DoF SVC-VV model
(c) Maximum of MSI by 6 DoF SVC model
(d) Maximum of MSI by 6 DoF SVC-VV model

Fig. 14. Mean and maximum MSI predicted by the 6 DoF SVC model and the 6 DoF SVC-VV model (error bar: 95% confidence interval).

TABLE V
TWO-WAY MIXED-DESIGN ANOVA FOR MEAN OF MSI PREDICTED BY 6 DOF SVC MODEL AND 6 DOF SVC-VV MODEL, SEPARATELY. ** SHOWS THE $p < .01$

Model	Source	SS	DF1	DF2	MS	*F-value*	*p-value*	η_p^2
6 DoF SVC model	Groups	7.100	1	25	7.100	1.526	0.228	0.058
	Conditions	6.696	1	25	6.696	2.846	0.104	0.102
	Interaction	6.841	1	25	6.841	2.907	0.101	0.104
6 DoF SVC-VV model	Groups	0.303	1	25	0.303	0.070	0.793	0.003
	Conditions	22.340	1	25	22.340	8.268	**0.008** **	0.249
	Interaction	11.113	1	25	11.113	4.113	0.053	0.141

TABLE VI
TWO-WAY MIXED-DESIGN ANOVA FOR MAXIMUM OF MSI PREDICTED BY 6 DOF SVC MODEL AND 6 DOF SVC-VV MODEL, SEPARATELY. ** SHOWS THE $p < .01$

Model	Source	SS	DF1	DF2	MS	*F-value*	*p-value*	η_p^2
6 DoF SVC model	Groups	30.681	1	25	30.681	1.566	0.222	0.059
	Conditions	22.482	1	25	22.482	2.664	0.115	0.096
	Interaction	28.149	1	25	28.149	3.336	0.080	0.118
6 DoF SVC-VV model	Groups	0.018	1	25	0.018	0.001	0.978	0.000
	Conditions	121.214	1	25	121.214	10.114	**0.004** **	0.288
	Interaction	44.914	1	25	44.914	3.748	0.064	0.130

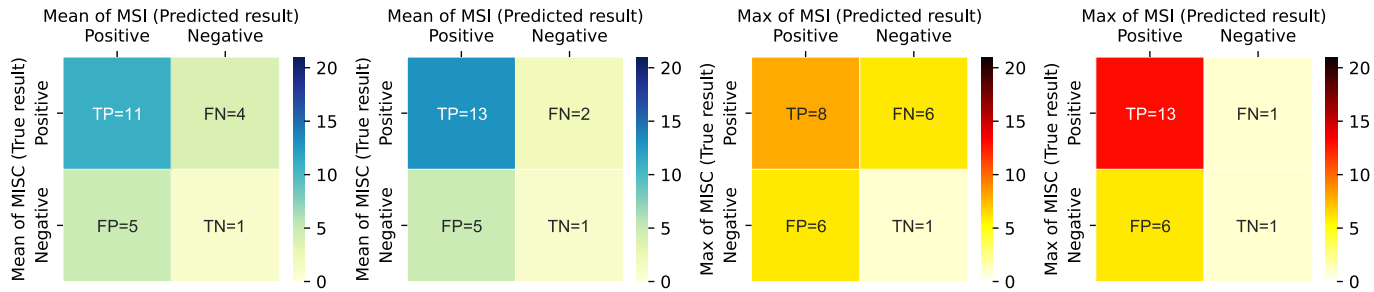

(a) Mean of MSI by 6 DoF SVC model
(b) Mean of MSI by 6 DoF SVC-VV model
(c) Maximum of MSI by 6 DoF SVC model
(d) Maximum of MSI by 6 DoF SVC-VV model

Fig. 15. Confusion matrices for the mean and maximum MSI predicted by 6 DoF SVC and 6 DoF SVC-VV models based on the mean and maximum MISC reported from 21 participants who felt symptoms of motion sickness in at least one of the riding conditions. As the true result, the mean of MISC had 15 positive cases and 6 negative cases; the Maximum of MISC had 14 positive cases and 7 negative cases.

predicted MSI was difficult to represent the individual features of participants who did not suffer from motion sickness. Therefore, in the analysis in this subsection, we excluded data from these six participants.

By analyzing the MISC of the remaining 21 participants, the mean MISC had 15 positive cases and 6 negative cases; the maximum MISC had 14 positive cases and 7 negative cases. Taking the MISC results as the true result, confusion matrices

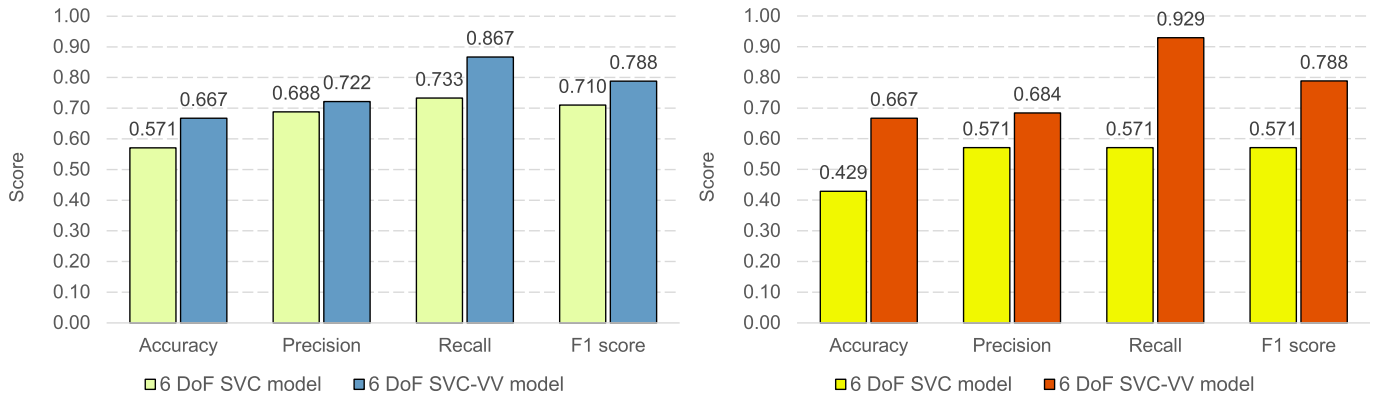

(a) Mean of MSI

(b) Maximum of MSI

Fig. 16. Accuracy, precision, recall, and F1 score for the mean and maximum MSI predicted by the 6 DoF SVC and 6 DoF SVC-VV models based on the mean and maximum MISC reported from 21 participants who felt symptoms of motion sickness in at least one of the riding conditions.

of the mean and maximum MSI predicted by the 6 DoF SVC and 6 DoF SVC-VV models are shown in Fig. 15. Regardless of whether for the mean or maximum MSI, the TP when using the 6 DoF SVC-VV model was higher than that when using the 6 DoF SVC-VV; however, the TN when using the 6 DoF SVC-VV model was lower than that when using the 6 DoF SVC model.

Based on these confusion matrices, the scores of accuracy, precision, recall, and F1-score for the mean and maximum MSI predicted by the 6 DoF SVC and 6 DoF SVC-VV models are shown in Fig. 16. Both the mean and maximum MSI predicted using the 6 DoF SVC-VV model had higher scores for accuracy, precision, recall, and F1 score than those predicted using the 6 DoF SVC model. However, the difference between the precision scores of the mean and maximum MSI when these two models were used was small.

VI. Discussions

A. Reported MISC

The MISC reported by 27 participants at each minute is shown in Fig. 12. We found that 21 of the 27 participants experienced motion sickness symptoms during the APMV riding experiment. This result illustrates that although APMVs are driven at a lower speed than vehicles, their passengers also have a high risk of motion sickness when it frequently avoids obstacles or other pedestrians. However, many other studies have reported that passengers are prone to motion sickness when using cars [40], [41], [42]. or other vehicles, such as vessels [43], [44], and aircrafts [45], we reported unprecedented results of motion sickness in passengers when using miniaturized autonomous vehicles, such as APMV. Therefore, this study presents a novel issue regarding motion sickness and a new mindset for improving passenger ride comfort for researchers and manufacturers of miniaturized autonomous vehicles.

As presented in Table IV, we did not find a significant effect of the experimental order of LAD and WAD on the MISC results based on the between-group design. For the within-group design, the results of the statistical tests validated our hypothesis $\boldsymbol{H}$ in participants working with a tablet device on the APMV (WAD) produced significantly more profound motion sickness symptoms than when looking ahead (LAD) (Fig. 10 and Table IV). This result is consistent with the conclusions of [14], [15], [46], [47], [48], and [49], where motion sickness is induced by visual obstruction when passengers ride in a car. One potential solution to reduce the motion sickness, which involves difficulty in passengers obtaining information about the vertical direction from their vision, is to consider filling in the missing visual vertical cues [48], [50].

Furthermore, we found that, in Fig. 10, the degree of motion sickness symptoms differed among participants. Such individual differences in motion sickness susceptibility were also reported in [49] and [51]. Although this study aimed to model motion sickness to predict MSI, considering these individual differences in the 6 DoF SVC-VV model is a challenging future work.

B. Calculated Visual Vertical

The calculated visual vertical directions θ^{vv} by the proposed method were compared with the gravitational acceleration directions θ^{g} which were estimated from the measured acceleration ($\boldsymbol{f} = \boldsymbol{g} + \boldsymbol{a}$) by IMU attached to the participant's head. The results in Fig. 11 show that the mean of the correlation coefficients under the LAD condition was significantly higher than their correlation coefficients under the WAD condition, suggesting that the proposed visual vertical prediction method can: 1) calculate the visual vertical direction from environmental images with correlation to the direction of gravitational acceleration in the absence of visual occlusion; 2) represent the effect of visual occlusion on the prediction of visual vertical information from environmental images, e. g., participants look-ahead and look-at-the-tablet device in an indoor environment.

This conclusion is consistent with the results of our previous study [13], which focused on the use of APMV under outdoor conditions. However, the correlation coefficients between the calculated visual vertical direction and gravitational acceleration direction in this experiment were not as high as those in our previous study. Two reasons can be considered:1) The

experimental scenes in this study were indoors; thus, the contours of the objects affected the visual vertical prediction, e. g., , tables and chairs placed in different directions. In [13], the horizon line and contours of buildings in an open scene contribute to the prediction of the visual vertical direction. 2) There was noise in estimating gravitational acceleration owing to the movement of APMV. In [13], the calculated visual vertical directions were evaluated with the direction of acceleration $\boldsymbol{f}$ under a static condition (APMV was stopped, $\boldsymbol{a} = [0, 0, 0]^T$), in which measured acceleration $\boldsymbol{f} = \boldsymbol{g}$, whereas the present study used an acceleration signal, which is composed of the summation of inertial acceleration and gravitational acceleration, i. e., $\boldsymbol{f} = \boldsymbol{g} + \boldsymbol{a}$.

C. Predicted MSI

The conventional 6 DoF SVC and 6 DoF SVC-VV models were used to predict MSI from IMU and camera data from 27 participants (Fig. 14).

As previously explained, MSI and MISC are different indicators for evaluating motion sickness, i. e., MSI indicates the percentage of participants experiencing vomiting when exposed to motion for a certain time; MISC indicates each participant's subjective assessment of the severity of motion sickness. Compared to the MISC reported in Fig. 12, the predicted MSI cannot represent the individual differences in motion sickness susceptibility.

In a between-group design, the results in Tables V and VI show that the mean and maximum of the predicted MSI using the two models were not significantly different between the groups, that is, the order of LAD and WAD, is consistent with the MISC results (see Table IV).

In a within-group design, the mean and maximum of the predicted MSI using the 6 DoF SVC model showed no significant difference between the LAD and WAD conditions. This is inconsistent with the MISC results because the MISC in WAD is significantly higher than that in LAD (see Table IV). Contrarily, the proposed 6 DoF SVC-VV model predicted a significantly higher MSI under WAD than under LAD with the same trend as the MISC reported by the participants (see Fig. 10 and Table IV). This implies that adding a visual vertical part to the conventional vestibular motion sickness 6DOF-SVC model facilitates the description of the difference in motion sickness under different visual conditions.

In summary, the results obtained in this study imply that the proposed 6 Dof SVC-VV model can describe the difference in the severity of motion sickness for different vertical visual conditions, such as increased motion sickness when reading books during APMV while the conventional 6 Dof SVC model does not.

D. Comparison Between the Predicted MSI and the Reported MISC

In this subsection, we discuss the performance of the predicted MSI by comparing it with the reported MISC.

Figure 15 shows the confusion matrices for the mean and Maximum of MSI predicted by the 6 DoF SVC and the 6 DoF SVC-VV models based on the mean and Maximum of MISC reported by 21 participants (excluding six participants who did not have any motion sickness symptoms). The mean of MSI (Fig. 15 (a) and (b)), when using 6 Dof SVC-VV model, TP=13 was higher than when using 6 Dof SVC model, i. e., TP=11. Similarly, the TP cases of the maximum MSI using the 6 Dof SVC-VV model was 13, which was also higher than the TP=8 obtained using the 6 Dof SVC model. Moreover, for both the mean and maximum of MSI, the number of correctly predicted negative cases (TN) by the 6 Dof SVC-VV model was same as when using the 6 Dof SVC model.

Based on the confusion matrices above, the accuracy, precision, recall, and F1 score for the mean and Maximum of MSI predicted by the 6 DoF SVC and 6 DoF SVC-VV models are shown in Fig. 16. The accuracy and F1 score are the overall evaluations of the prediction results. The accuracy and F1 scores of the 6 DoF SVC-VV model were higher than those of the 6 DoF SVC model for both the mean and maximum values of the MSI. Moreover, precision and recall are sub-scores of the F1 score. For both the mean and maximum of the MSI, the precision scores of the 6 DoF SVC-VV and 6 DoF SVC models were similar; however, the recall scores of the 6 DoF SVC-VV model were higher than those of the 6 DoF SVC model. Based on Table III, both models had the same performance in predicting the correct positive results over all positive predictions; however, the 6 DoF SVC-VV model had a better performance in predicting correct positive results over all positive true results.

E. Limitations

The visual vertical prediction method proposed in this study can only predict the visual vertical direction in a 2D plane. Therefore, the visual vertical direction changes caused by head rotations along the pitch axis cannot yet be calculated.

The parameters in Table I were obtained from the conventional 6 DoF SVC model of a previous study [24], which did not include visual-vestibular interaction. Therefore, these parameters may not be optimal for the proposed 6 DoF SVC-VV model.

All participants were in their 20s. A broader demographic survey is necessary, particularly for the elderly, who are potential wheelchair users.

Furthermore, the proposed 6 DoF SVC-VV model cannot be used to represent the individual traits of motion sickness susceptibility because this model is designed to predict MSI. Particularly, it is difficult to apply this model to people who are extremely insensitive to motion sickness.

F. Future Works

The visual vertical prediction method was improved to extract 3D visual vertical features from image data. This will further help the 6 DoF SVC-VV model represent the change in the visual vertical direction owing to head rotations on the pitch axis.

Although the 6 DoF SVC-VV model uses the parameters optimized by Inoue et al. [24], the study of [52] pointed out that the parameters of the 6 DoF SVC model need to be further optimized in order to represent different kinds of motion sickness observations. In addition, the new parameter K_{vvc}, which is the feedback gain of the visual vertical conflict, has

not yet been optimized. We will address this issue in future studies by adjusting parameters of the 6 DoF SVC-VV model to match the full range of motion sickness observations.

Furthermore, because the proposed 6 DoF SVC-VV model cannot be used to represent the individual traits of motion sickness susceptibility, we will develop a new MISC prediction model based on the 6 DoF SVC-VV model based on the model proposed in [49].

Moreover, we consider that working with a tablet device during riding APMV hinders the visual vertical perception of passengers and their motion perception through dynamic vision. Therefore, the integration of the proposed 6 DoF SVC-VV model with the visual flow, referring to Wada et al. [27], is an important future direction.

We have noted that different vehicles, such as cars, trains, airplanes, etc., exhibit specific motion amplitudes. Therefore, determining the motion frequencies and amplitudes at which visual occlusion is more likely to induce motion sickness in passengers is indeed a significant focus area for our future work.

VII. Conclusion

To model motion sickness in passengers under different visual conditions while using the APMV, this study proposes a new computational model of SVC theory for predicting motion sickness that considers the interactions between vertical perception from the visual and vestibular systems. We added a module for visual vertical perception to the 6 DoF SVC model in [24]. Therefore, we proposed a visual vertical prediction method based on an image processing technique.

In the experiment, 27 participants experienced APMV with two visual conditions: looking ahead (LAD) and working with a tablet device (WAD). Of these, 21 participants reported motion sickness symptoms, particularly in the WAD condition. Furthermore, based on the MISC reported by the participants, we found that the proposed 6 DoF SVC-VV model more accurately predicted MSI than the conventional 6 DoF SVC model without visual input when the visual vertical direction and direction of gravitational acceleration differed, such as when participants worked with a tablet device while using an APMV.

CRediT Authorship Contribution Statement

Hailong Liu: conceptualization, investigation, resources, methodology, validation, formal analysis, visualization, writing—original draft, and writing—review & editing.

Shota Inoue: conceptualization, methodology, and writing—review & editing.

Takahiro Wada: conceptualization, methodology, writing—review & editing, project administration, and funding acquisition.

References

[1] *Taxonomy and Definitions for Terms Related to Driving Automation Systems for On-Road Motor Vehicles*, SAE Tech. Standard J3016b, 2018, pp. 1–35.

[2] Y. Morales, T. Miyashita, and N. Hagita, "Social robotic wheelchair centered on passenger and pedestrian comfort," *Robot. Auto. Syst.*, vol. 87, pp. 355–362, Jan. 2017.

[3] H. Liu, T. Hirayama, L. Y. M. Saiki, and H. Murase, "What timing for an automated vehicle to make pedestrians understand its driving intentions for improving their perception of safety?" in *Proc. IEEE 23rd Int. Conf. Intell. Transp. Syst. (ITSC)*, Sep. 2020, pp. 1–6.

[4] Y. Kobayashi et al., "Robotic wheelchair easy to move and communicate with companions," in *Proc. CHI Extended Abstr. Human Factors Comput. Syst.* New York, NY, USA: Association for Computing Machinery, Apr. 2013, pp. 3079–3082.

[5] S. Ali, A. Lam, H. Fukuda, Y. Kobayashi, and Y. Kuno, "Smart wheelchair maneuvering among people," in *Proc. Int. Conf. Intell. Comput.* Cham, Switzerland: Springer, 2019, pp. 32–42.

[6] H. Liu, T. Hirayama, L. Y. M. Saiki, and H. Murase, "Implicit interaction with an autonomous personal mobility vehicle: Relations of pedestrians' gaze behavior with situation awareness and perceived risks," *Int. J. Hum. Comput. Interact.*, vol. 39, no. 10, pp. 1–17, May 2022.

[7] M. Sivak and B. Schoettle, "Motion sickness in self-driving vehicles," Univ. Michigan, Transp. Res. Inst., Ann Arbor, MI, USA, Tech. Rep. UMTRI-2015-12, 2015. [Online]. Available: https://deepblue.lib.umich.edu/handle/2027.42/111747

[8] T. Wada, "Motion sickness in automated vehicles," in *Proc. 13th Int. Symp. Adv. Vehicle Control*, 2016, pp. 169–174.

[9] C. Diels and J. E. Bos, "Self-driving carsickness," *Appl. Ergonom.*, vol. 53, pp. 374–382, Mar. 2016.

[10] Y. Li, H. Liu, and B. Deml, "HMI-based communication methods for negotiation between a manually driven vehicle driver and an autonomous vehicle in an ambiguous traffic scenario," in *Proc. IEEE/SICE Int. Symp. Syst. Integr. (SII)*, Jan. 2022, pp. 244–249.

[11] N. Isu, T. Hasegawa, I. Takeuchi, and A. Morimoto, "Quantitative analysis of time-course development of motion sickness caused by in-vehicle video watching," *Displays*, vol. 35, no. 2, pp. 90–97, Apr. 2014.

[12] H. Sato, Y. Sato, A. Takamatsu, M. Makita, and T. Wada, "Earth-fixed books reduce motion sickness when reading with a head-mounted display," *Frontiers Virtual Reality*, vol. 3, pp. 1–9, May 2022. [Online]. Available: https://www.frontiersin.org/articles/10.3389/frvir.2022.909005/full

[13] H. Liu, S. Inoue, and T. Wada, "Motion sickness modeling with visual vertical estimation and its application to autonomous personal mobility vehicles," in *Proc. IEEE Intell. Vehicles Symp. (IV)*, Jun. 2022, pp. 1415–1422.

[14] K. Kato and S. Kitazaki, "A study of carsickness of rear-seat passengers due to acceleration and deceleration when watching an in-vehicle display," *Rev. Automot. Eng.*, vol. 27, no. 3, pp. 465–469, Jul. 2006.

[15] O. X. Kuiper, J. E. Bos, and C. Diels, "Looking forward: In-vehicle auxiliary display positioning affects carsickness," *Appl. Ergonom.*, vol. 68, pp. 169–175, Apr. 2018.

[16] J. Li, A. Reda, and A. Butz, "Queasy rider: How head movements influence motion sickness in passenger use of head-mounted displays," in *Proc. 13th Int. Conf. Automot. User Interfaces Interact. Veh. Appl.*, Sep. 2021, pp. 28–38.

[17] Y. Li, H. Cheng, Z. Zeng, H. Liu, and M. Sester, "Autonomous vehicles drive into shared spaces: EHMI design concept focusing on vulnerable road users," in *Proc. IEEE Int. Intell. Transp. Syst. Conf. (ITSC)*, Sep. 2021, pp. 1729–1736.

[18] J. Iskander et al., "From car sickness to autonomous car sickness: A review," *Transp. Res. F, Traffic Psychol. Behaviour*, vol. 62, pp. 716–726, Apr. 2019.

[19] J. T. Reason, "Motion sickness adaptation: A neural mismatch model," *J. Roy. Soc. Med.*, vol. 71, no. 11, pp. 819–829, Nov. 1978.

[20] C. M. Oman, "Motion sickness: A synthesis and evaluation of the sensory conflict theory," *Can. J. Physiol. Pharmacol.*, vol. 68, no. 2, pp. 294–303, Feb. 1990.

[21] W. Bles, J. E. Bos, B. de Graaf, E. Groen, and A. H. Wertheim, "Motion sickness: Only one provocative conflict?" *Brain Res. Bull.*, vol. 47, no. 5, pp. 481–487, Nov. 1998.

[22] J. E. Bos and W. Bles, "Modelling motion sickness and subjective vertical mismatch detailed for vertical motions," *Brain Res. Bull.*, vol. 47, no. 5, pp. 537–542, Nov. 1998.

[23] N. Kamiji, Y. Kurata, T. Wada, and S. Doi, "Modeling and validation of carsickness mechanism," in *Proc. SICE Annu. Conf.*, Sep. 2007, pp. 1138–1143.

[24] S. Inoue, H. Liu, and T. Wada, "Revisiting motion sickness models based on SVC theory considering motion perception," SAE Tech. Paper 2023-01-0176, 2023. [Online]. Available: https://www.sae.org/publications/technical-papers/content/2023-01-0176/

[25] J. E. Bos, W. Bles, and E. L. Groen, "A theory on visually induced motion sickness," *Displays*, vol. 29, no. 2, pp. 47–57, Mar. 2008.

[26] C. Braccesi and F. Cianetti, "Motion sickness—Part I: Development of a model for predicting motion sickness incidence," *Int. J. Human Factors Model. Simul.*, vol. 2, no. 3, pp. 163–187, 2011.

[27] T. Wada, J. Kawano, Y. Okafuji, A. Takamatsu, and M. Makita, "A computational model of motion sickness considering visual and vestibular information," in *Proc. IEEE Int. Conf. Syst., Man, Cybern. (SMC)*, Oct. 2020, pp. 1758–1763.

[28] L. Yardley, "Motion sickness susceptibility and the utilisation of visual and otolithic information for orientation," *Eur. Arch. Oto-Rhino-Laryngol.*, vol. 247, no. 5, pp. 300–304, Jul. 1990.

[29] P. L. Michelson, D. L. McCaslin, G. P. Jacobson, M. Petrak, L. English, and K. Hatton, "Assessment of subjective visual vertical (SVV) using the 'bucket test' and the virtual SVV system," *Amer. J. Audiol.*, vol. 27, no. 3, pp. 249–259, 2018.

[30] M. Guerraz, "Visual vertigo: Symptom assessment, spatial orientation and postural control," *Brain*, vol. 124, no. 8, pp. 1646–1656, Aug. 2001.

[31] T. K. Clark, M. C. Newman, F. Karmali, C. M. Oman, and D. M. Merfeld, "Mathematical models for dynamic, multisensory spatial orientation perception," *Prog. Brain Res.*, vol. 248, pp. 65–90, Jan. 2019.

[32] D. Merfeld, "Modeling the vestibulo-ocular reflex of the squirrel monkey during eccentric rotation and roll tilt," *Exp. Brain Res.*, vol. 106, no. 1, pp. 123–134, Sep. 1995.

[33] J. E. Bos and W. Bles, "Theoretical considerations on canal-otolith interaction and an observer model," *Biol. Cybern.*, vol. 86, no. 3, pp. 191–207, Mar. 2002.

[34] T. Wada, "Computational model of motion sickness describing the effects of learning exogenous motion dynamics," *Frontiers Syst. Neurosci.*, vol. 15, p. 6, Feb. 2021.

[35] M. Jeannerod, *Motor Cognition: What Actions Tell the Self*, vol. 42. Oxford, U.K.: Oxford Univ. Press, 2006.

[36] G. Wetzstein, *Virtual Reality Course Notes: 3-DOF Orientation Tracking with IMUs*, document EE 267, 2017.

[37] M. McCauley, J. Royal, C. Wylie, J. O'Hanlon, and R. Mackie, "Motion sickness incidence: Exploratory studies of habituation, pitch and roll, and the refinement of a mathematical model," Office Naval Res., Hum. Factors Res., Arlington, VA, USA, Tech. Rep. 1733-2, 1976.

[38] A. Watanabe, D. Endo, G. Yamauchi, and K. Nagatani, "Neonavigation meta-package: 2-D/3-DOF seamless global–local planner for ROS—Development and field test on the representative offshore oil plant," in *Proc. IEEE Int. Symp. Saf., Secur., Rescue Robot. (SSRR)*, Oct. 2016, pp. 86–91.

[39] J. E. Bos, S. N. MacKinnon, and A. Patterson, "Motion sickness symptoms in a ship motion simulator: Effects of inside, outside, and no view," *Aviation, Space, Environ. Med.*, vol. 76, no. 12, pp. 1111–1118, 2005.

[40] M. Turner, "Motion sickness in public road transport: Passenger behaviour and susceptibility," *Ergonomics*, vol. 42, no. 3, pp. 444–461, Mar. 1999.

[41] T. Wada, H. Konno, S. Fujisawa, and S. Doi, "Can passengers' active head tilt decrease the severity of carsickness? Effect of head tilt on severity of motion sickness in a lateral acceleration environment," *Human Factors, J. Human Factors Ergonom. Soc.*, vol. 54, no. 2, pp. 226–234, Apr. 2012.

[42] A. Brietzke, R. P. Xuan, A. Dettmann, and A. C. Bullinger, "Influence of dynamic stimulation, visual perception and individual susceptibility to car sickness during controlled stop-and-go driving," *Forschung Ingenieurwesen*, vol. 85, no. 2, pp. 517–526, Jun. 2021.

[43] R. L. Pepper and S. F. Wiker, "Repeated assessment of stress, mood and performance changes resulting from exposure to vessel motions at sea," in *Proc. Human Factors Soc. Annu. Meeting*, vol. 23, no. 1. Los Angeles, CA, USA: SAGE Publications, 1979, pp. 549–553.

[44] O. Turan, C. Verveniotis, and H. Khalid, "Motion sickness onboard ships: Subjective vertical theory and its application to full-scale trials," *J. Mar. Sci. Technol.*, vol. 14, no. 4, pp. 409–416, Dec. 2009.

[45] O. Samuel and D. Tal, "Airsickness: Etiology, treatment, and clinical importance—A review," *Mil. Med.*, vol. 180, no. 11, pp. 1135–1139, Nov. 2015.

[46] M. J. Griffin and M. M. Newman, "Visual field effects on motion sickness in cars," *Aviation, Space, Environ. Med.*, vol. 75, no. 9, pp. 739–748, 2004.

[47] J. Karjanto, N. M. Yusof, C. Wang, J. Terken, F. Delbressine, and M. Rauterberg, "The effect of peripheral visual feedforward system in enhancing situation awareness and mitigating motion sickness in fully automated driving," *Transp. Res. F, Traffic Psychol. Behaviour*, vol. 58, pp. 678–692, Oct. 2018.

[48] T. Suwa, Y. Sato, and T. Wada, "Reducing motion sickness when reading with head-mounted displays by using see-through background images," *Frontiers Virtual Reality*, vol. 3, p. 72, Jun. 2022.

[49] T. Irmak, D. M. Pool, and R. Happee, "Objective and subjective responses to motion sickness: The group and the individual," *Exp. Brain Res.*, vol. 239, no. 2, pp. 515–531, Feb. 2021.

[50] P. J. Feenstra, J. E. Bos, and R. N. H. W. van Gent, "A visual display enhancing comfort by counteracting airsickness," *Displays*, vol. 32, no. 4, pp. 194–200, Oct. 2011.

[51] J. F. Golding, "Predicting individual differences in motion sickness susceptibility by questionnaire," *Personality Individual Differences*, vol. 41, no. 2, pp. 237–248, Jul. 2006.

[52] T. Irmak, D. M. Pool, K. N. de Winkel, and R. Happee, "Validating models of sensory conflict and perception for motion sickness prediction," *Biol. Cybern.*, vol. 117, no. 3, pp. 185–209, Mar. 2023.

Hailong Liu (Member, IEEE) received the M.Eng. and Ph.D. degrees in engineering from the Graduate School of Information Science and Engineering, Ritsumeikan University, Japan, in 2015 and 2018, respectively. Meanwhile, he was a Research Fellowship of Young Scientists (DC2) of JSPS from April 2016 to March 2018. From April 2018 to October 2021, he was a Researcher with Nagoya University, Japan. He is currently an Assistant Professor with the Graduate School of Science and Technology, NAIST, Japan. His research has focused on human factors and machine learning in the intelligent transportation systems. He is a member of JSAE, JSAI, and SICE. He received the IEEE Intelligent Vehicles Symposium (IV) Best Student Paper Award in 2015 and the IEEE Global Conference on Consumer Electronics (IEEE GCCE) Outstanding Paper Award in 2016.

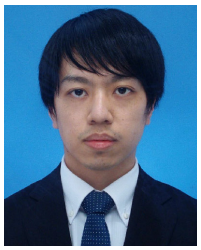

Shota Inoue received the bachelor's degree in engineering from the Akashi College, National Institute of Technology, Japan, in 2021. He is currently pursuing the master's degree with the Graduate School of Science and Technology, NAIST, Japan. His research has focused on modeling of motion sickness. He is a member of JSAE.

Takahiro Wada (Member, IEEE) received the B.S. degree in mechanical engineering, the M.S. degree in information science and systems engineering, and the Ph.D. degree in robotics from Ritsumeikan University, Japan, in 1994, 1996, and 1999, respectively. In 1999, he became a Research Associate with Ritsumeikan University. He spent 12 years with the Department of Intelligent Mechanical Systems Engineering, Kagawa University, Takamatsu, Japan, as an Assistant Professor and an Associate Professor. He has been a Full Professor for nine years with the College of Information Science and Engineering, Ritsumeikan University, since 2012. Since 2021, he has been a Full Professor with the Nara Institute of Science and Technology, Ikoma, Nara, Japan. In 2006 and 2007, he spent half a year with the Transportation Research Institute, University of Michigan, Ann Arbor, as a Visiting Researcher. His current research interests include robotics, human–machine systems, and human modeling, such as modeling motion sickness and motion perception.